Contrib Mineral Petrol (2016) 171:15
DOI 10.1007/s00410-015-1226-4

ORIGINAL PAPER

Dating prograde fluid pulses during subduction by in situ U–Pb and oxygen isotope analysis

Laure Gauthiez-Putallaz[1] · Daniela Rubatto[1,2] · Jörg Hermann[1,2]

Received: 26 July 2015 / Accepted: 30 December 2015 / Published online: 23 January 2016

Abstract The Dora-Maira whiteschists derive from metasomatically altered granites that experienced ultrahigh-pressure metamorphism at ~750 °C and 40 kbar during the Alpine orogeny. In order to investigate the P–T–time–fluid evolution of the whiteschists, we obtained U–Pb ages from zircon and monazite and combined those with trace element composition and oxygen isotopes of the accessory minerals and coexisting garnet. Zircon cores are the only remnants of the granitic protolith and still preserve a Permian age, magmatic trace element compositions and $\delta^{18}O$ of ~10 ‰. Thermodynamic modelling of Si-rich and Si-poor whiteschist compositions shows that there are two main fluid pulses during prograde subduction between 20 and 40 kbar. In Si-poor samples, the breakdown of chlorite to garnet + fluid occurs at ~22 kbar. A first zircon rim directly overgrowing the cores has inclusions of prograde phlogopite and HREE-enriched patterns indicating zircon growth at the onset of garnet formation. A second main fluid pulse is documented close to peak metamorphic conditions in both Si-rich and Si-poor whiteschist when talc + kyanite react to garnet + coesite + fluid. A second metamorphic overgrowth on zircon with HREE depletion was observed in the Si-poor whiteschists, whereas a single metamorphic overgrowth capturing phengite and talc inclusions was observed in the Si-rich whiteschists. Garnet rims, zircon rims and monazite are in chemical and isotopic equilibrium for oxygen, demonstrating that they all formed at peak metamorphism at 35 Ma as constrained by the age of monazite (34.7 ± 0.4 Ma) and zircon rims (35.1 ± 0.8 Ma). The prograde zircon rim in Si-poor whiteschists has an age that is within error indistinguishable from the age of peak metamorphic conditions, consistent with a minimum rate of subduction of 2 cm/year for the Dora-Maira unit. Oxygen isotope values for zircon rims, monazite and garnet are equal within error at 6.4 ± 0.4 ‰, which is in line with closed-system equilibrium fractionation during prograde to peak temperatures. The resulting equilibrium $\Delta^{18}O_{zircon\text{-}monazite}$ at 700 ± 20 °C is 0.1 ± 0.7 ‰. The in situ oxygen isotope data argue against an externally derived input of fluids into the whiteschists. Instead, fluid-assisted zircon and monazite recrystallisation can be linked to internal dehydration reactions during prograde subduction. We propose that the major metasomatic event affecting the granite protolith was related to hydrothermal seafloor alteration post-dating Jurassic rifting, well before the onset of Alpine subduction.

Keywords High-pressure fluids · Whiteschists · U–Pb dating · Oxygen isotopes · Ion microprobe · Metasomatism

Communicated by Dr. Othmar Müntener.

Electronic supplementary material The online version of this article (doi:10.1007/s00410-015-1226-4) contains supplementary material, which is available to authorized users.

✉ Laure Gauthiez-Putallaz
laure.gauthiez-putallaz@anu.edu.au

[1] Research School of Earth Sciences, The Australian National University, Canberra, ACT 0200, Australia

[2] Institute of Geological Sciences, University of Bern, 3012 Bern, Switzerland

Introduction

The subduction of crustal material to mantle depths and its chemical modification during burial and exhumation contribute to element recycling in the mantle and the formation of new crust through arc magmatism. Crustal rocks that

are subducted to ultrahigh-pressure conditions (UHP, >~30 kbar) and are exhumed back to the surface provide a rare window into such deep Earth processes. Exhumed UHP rocks offer the opportunity to study fluids at sub-arc depths, where such fluids facilitate significant crust–mantle mass transfer of major and trace elements (Tatsumi and Eggins 1995; Manning 2004; Hermann and Rubatto 2014). UHP fluids have been mostly investigated through fluid inclusions (e.g. Zhang et al. 2008; Ferrando et al. 2009; Frezzotti et al. 2011) or metamorphic veins (Zheng 2009; John et al. 2012). In samples that underwent extensive metasomatism, oxygen isotopes can assist in defining the source of the fluids (Zheng et al. 2003). With the capability to analyse oxygen isotopes in situ, it is now possible to retrieve information regarding the oxygen isotopic composition of the mineral zones at the same scale as U–Pb dating and trace element analysis. This allows reconstructing P–T–time–fluid evolutions in complex metamorphic rocks (Page et al. 2010, 2014; Martin et al. 2011, 2014; Rubatto and Angiboust 2015).

Dating of prograde fluid pulses that are related to the breakdown of hydrous phases is a difficult task. Pollington and Baxter (2010) and Dragovic et al. (2012) showed that prograde fluid release in subducted rocks can be dated with the Sm–Nd and Lu–Hf methods by carefully selecting garnet domains that result from dehydration reactions. However, the likely resetting of the Sm–Nd or Lu–Hf system above 700 °C (Philippot et al. 2001) hampers its use in many UHP terranes. Zircon and monazite also have the potential to recrystallise during prograde metamorphism and are readily datable using micro-analytical techniques. The age of different monazite/zircon growth zones can potentially be linked to different stages of metamorphism using inclusions and trace elements thus allowing the reconstruction of P–T–time paths for UHP rocks (e.g. Hermann et al. 2001; Rubatto 2002; Liu and Liou 2011; Gilotti 2013). With in situ oxygen isotope analyses of zircon and monazite domains, it is thus possible to additionally constrain the composition of fluids that were present during metamorphic stages.

One key question regarding the dynamics of UHP rocks is related to rates of subduction. The timing of exhumation of UHP units is relatively well known, as decreasing temperature during exhumation leads to the sequential closure of multiple radiogenic systems. Exhumation rates of UHP terranes is variable (Kylander-Clark et al. 2012; Hermann and Rubatto 2014): it has been proposed that smaller units as those found within the Western Alps (e.g. Lago di Cignana and Dora-Maira) undergo a fast exhumation cycle (of a few to ~10 Ma, Amato et al. 1999; Rubatto and Hermann 2001; Lapen et al. 2003), whereas larger UHP terranes record a more protracted history spanning over tens of million years (e.g. Dabie Sulu or Western Gneiss Region, Liu and Liou 2011; Schmidt et al. 2011). The rates at which such units are brought to depth are harder to constrain and rely on formation of prograde datable minerals, such as zircon, monazite or garnet, which can survive peak and retrograde equilibration (e.g. Skora et al. 2015). However, it has been recently proposed, based on Zr mass balance of rock-forming minerals, that new growth of zircon in UHP rocks is far more often related to retrograde than prograde metamorphism (Kohn et al. 2015). On the other hand, in fluid-rich systems where zircon dissolution and precipitation are dominant processes, formation of metamorphic zircon when prograde fluid release is expected (Rubatto and Hermann 2003; Geisler et al. 2007).

In this paper, we perform a detailed investigation of zircon and monazite behaviour during prograde dehydration reactions in the classical Dora-Maira UHP whiteschists, Western Alps. By combining U–Pb, oxygen isotopes and trace element micro-analysis of distinct mineral zones, together with thermodynamic modelling, we aim at reconstructing the prograde P–T–time–fluid path of the UHP Dora-Maira whiteschists. This information is used to constrain subduction rates of the UHP unit and to gain information on the sources and timing of fluid–rock interaction.

Geological background

The Dora-Maira whiteschists outcrop in the Brossasco-Isasca unit of the Western Alps, Italy. This unit is composed of a basement that underwent amphibolite facies metamorphism during the Variscan orogeny and was later intruded by Permian granites (Gebauer et al. 1997) that constitute a monometamorphic complex (Compagnoni and Hirajima 2001; Compagnoni et al. 2012). The unit underwent Alpine metamorphism in the Late Eocene to Early Oligocene (Gebauer et al. 1997; Rubatto and Hermann 2001).

The Dora-Maira whiteschists are key samples for the understanding of UHP metamorphism as 40 years of previous studies covering mineralogy, petrology, thermobarometry and fluid inclusions allow an extraordinary level of depth in interpretations of new data. The Dora-Maira whiteschists are the type locality for UHP metamorphism (Chopin 1984) and preserve extreme metamorphic conditions up to the diamond stability field (Hermann 2003). The whiteschists (Schreyer 1973) are also referred to as pyrope quartzite (Chopin and Monié 1984) and form lenses and layers of talc–phengite–kyanite–pyrope–quartz–coesite schists within a metagranite. The whiteschists have a peculiar chemistry characterised by average SiO_2 of 65–75 wt% and K_2O of 2–2.5 %, are strongly enriched in Mg and depleted in Fe^{2+}, Na and Ca (their chemistry is close to the KMASH system, e.g. Chopin and Schertl 1999). For most elements, the trace element signature of the whiteschists is similar to that of the surrounding metagranite (Schertl and

Schreyer 2008), but they are depleted in Zn, Rb, Ba, Sr and P. Previous authors (Compagnoni and Hirajima 2001; Ferrando et al. 2009) proposed that the whiteschists' composition resulted from pervasive metasomatism during subduction, with important implications for fluid migration at depth in the subduction zone.

The relatively simple composition of the whiteschists provides an excellent basis to compare observed mineral assemblages and compositions to experimentally determined phase relations. Schertl et al. (1991) proposed peak metamorphic conditions of 750 °C and 37 kbar. Later, slightly higher peak pressures of ~43 kbar were postulated (Simon et al. 1997; Hermann 2003). Main retrograde decompression stages through 700–670 °C, 30–25 kbar and 600 °C, 11 kbar are associated with the influx of minor amounts of fluid.

Gebauer et al. (1997) pioneered ion microprobe U–Pb dating in high-pressure samples and showed that zircons in the whiteschists have cores of Permian age that are identical to the zircons in the surrounding metagranite. Rare zircon rims yield an age of 35.4 ± 1.0 Ma (Gebauer et al. 1997) dating UHP metamorphism, confirming earlier results by Tilton et al. (1991). Other minerals dated previously also yielded Alpine ages such as monazite at ~35 Ma (Vaggelli et al. 2006) and 30–34 Ma (Tilton et al. 1991), ellenbergerite at 30–34 Ma as well as pyropes that yield Sm/Nd ages of 34–38 Ma (Tilton et al. 1991). Whole rock–garnet Lu–Hf dating by Duchêne et al. (1997) provided an age of 32.8 ± 1.2 Ma attributed to the first stages of a fast exhumation. UHP titanite from a calc-silicate within the same unit also returned a U–Pb age of 35.1 ± 0.9 Ma, whereas low-pressure titanite constrained the exhumation to mid-crustal levels at 31.8 ± 0.5 Ma (Rubatto and Hermann 2001). These geochronological constrains allowed calculation of an initial fast exhumation rates of ~3.6 cm/year for the UHP unit (Rubatto and Hermann 2001).

Analytical methods

Trace elements were measured on an ArF excimer laser coupled to a quadrupole Inductively Coupled Plasma Mass Spectrometer (ICP-MS) Agilent 7700 at the Research School of Earth Sciences at the Australian National University (RSES at ANU), using the set-up described in Eggins et al. (1998). The laser was tuned to a frequency of 5 Hz and energy of 50 mJ (corresponding to a HV of around 26–27 kV). Spot sizes of 22 μm for zircon and monazite and of 62 μm for garnet were used. The counts were standardised to NIST 610 (zircon and monazite) and NIST 612 (garnet) glasses, and accuracy was monitored by analysing BCR-2G glass. Data were acquired over a 65 s analysis that included a 20 s background. The reference materials were measured after every eight unknowns. Stoichiometric Si was employed as internal standard for zircon (SiO_2: 31.6 wt%) and garnet (SiO_2: 44 wt%), whereas Th concentrations measured by electron microprobe (EMPA) were used for monazite. Reproducibility and accuracy as assessed on the BCR-2G glass were within 10 % or less across all analysed elements. The data were reduced with the freeware Iolite (Paton et al. 2011) and its data reduction scheme for trace elements (Woodhead et al. 2007). Accuracy and reproducibility of the secondary standard were generally within 10 % of the reference value.

EMPA analyses of monazites were performed at RSES using a Cameca SX100 with a current of 100 nA, acceleration voltage of 15 kV and a spot size of 1.5 μm. For REE analyses, Lα or Lβ peaks and background positions were carefully selected to minimise interferences. Al and Si were measured for 10 s on the first spectrometer (Sp1, TAP), and Y was measured for 30 s. On Sp2 (PET), Ca was measured for 10 s, P (20 s) and Y (30 s). On Sp3 (LPET), La was measured for 10 s on Lα, as well as U (60 s) on Mβ and Th (30 s) on Mα. On Sp4 (LLIF), Ce was measured for 10 s on Lα and the heavier REE for 30 s: Nd, Sm, Pr and Gd on Lβ; Dy, Er and Yb on Lα. Synthetic phosphates were used for the calibration of REE, synthetic oxides for Th and U, wollastonite for Ca, corundum for Al, apatite for P and quartz for Si. Trebilcock (J. Pyle) and 8153 (R. Stern) monazites were used as secondary standards, and our data agreed within error with the published values.

Back-scattered electron (BSE) as well as cathodoluminescence (CL) images were produced with a JEOL-JSM_6610A SEM, using an acceleration voltage of 15 kV and a working distance around 11 and 25 mm, respectively. Standardised EDS analyses were performed using a JEOL JSM-6400 at the Centre for Advanced Microscopy at ANU using 15 kV acceleration voltage, a beam current of 1 nA and 120 s of count acquisition, resulting in detection limits of 0.15–0.2 wt%. The precise spot location of the SEM is advantageous for the analyses of mineral inclusions in zircon (Hermann et al. 2001).

Zircon U–Pb dating was performed on the Sensitive High-Resolution Ion Microprobe SHRIMP II at RSES, according to the method described in Williams (1998). Standards and unknown were analysed with a spot size of around 20 × 25 μm. Temora zircon (417 Ma, Black et al. 2003) was used as standard for internal mass fractionation and U concentration (160 ppm). Monazites were analysed using a similar method as for zircon and standardised to USGS44069 monazite (424.9 ± 0.4 Ma, Aleinikoff et al. 2006). Energy filtering was used in order to exclude LREE-Hf molecule interferences on the Pb peaks and reduce ThO counts as described in Rubatto and Hermann (2001). The typical calibration errors were 1.5 % for the zircon and 1 % for the monazite sessions. Ratios

were corrected for common Pb according to the measured $^{207}Pb/^{206}Pb$ ($^{7/6}R_m$) and the non-radiogenic $^{207}Pb/^{206}Pb$ ($^{7}R_c$) following the method described in Williams (1998), i.e. $f_{206} = (^{7/6}R_m - {}^{7/6}R^*)/(^{7/6}R_c - {}^{7/6}R^*)$, where $^{7/6}R^*$ is the expected radiogenic $^{207}Pb/^{206}Pb$ assuming concordance at the approximate age of the sample. For zircon, the $^{7}R_c$ composition was assumed to be that predicted by Stacey and Kramers (1975) model, but in the case of monazite with high f_{206} the common Pb composition was regressed from the analyses (see details in result section). Data reduction was performed using MS Excel extensions SQUID 2.5 (Ludwig 2009) and Isoplot 4 (Ludwig 2012).

Zircon and monazite oxygen isotopes were analysed on the same mounts as U–Pb dating with the SHRIMP II instrument following the procedure described in Ickert et al. (2008) and Rubatto et al. (2014), respectively. Standards Temora (TEM, 8.2 ‰, Black et al. 2004) and USGS44069 (7.7 ‰, Rubatto et al. 2014) were used for zircon and monazite, respectively. The reproducibility of TEM zircons and USGS44069 monazite was within 0.5 ‰ (2σ) during each analytical session. Raw data were processed with the in-house software POXI. The monazite analyses were corrected for matrix effect according to the cheralite and huttonite substitutions, as proposed in Rubatto et al. (2014) using Si and Ca measured by EMPA near the SHRIMP spots.

Garnet oxygen isotopes have been measured on SHRIMP SI following the method of Martin et al. (2014). Two half garnets were cut out of the thin sections used for trace element analyses and were mounted alongside grain separates from the same samples and garnet standards UWG2 and PrPDM. Analyses consisted of 5 scans of 20 s for a total counting time of 100 s, and the standards were measured every 5 unknowns. The reproducibility of UWG2 and PrPDM was within 0.5 ‰ (2σ) for the analytical session. Error propagation for oxygen isotope analyses follows Martin et al. (2014). For sample averages, the uncertainty is calculated as the quadratic sum of the standard error of the mean of the standard measurements within that analytical session, the standard error on the laser fluorination value of the standard and the average uncertainty on individual analyses.

Results

Sample description

We investigated four samples of whiteschists and pyrope quartzite from the whiteschist lens that outcrop at the Case Parigi locality (Chopin 1984; Schertl and Schreyer 2008) and that were previously used for P–T calculations by Hermann (2003). DM1C has been sampled close to the border of the whiteschist lens and is of the SiO_2-rich type of Hermann (2003). It contains 50 % of quartz (retrogressed from peak coesite), small garnets (up to 1 cm in size) as well as phengite and kyanite (Fig. 1). Peak phengite is aligned along a weak foliation and is characterised by a high Si content per formula unit (pfu) of 3.6 (Hermann 2003). Accessory phases are abundant rutile, rare monazite and zircon, as well as inclusions of apatite and florencite in garnet. DM1C displays a small degree of retrogression with talc, kyanite and minor phlogopite forming at the rims of garnet.

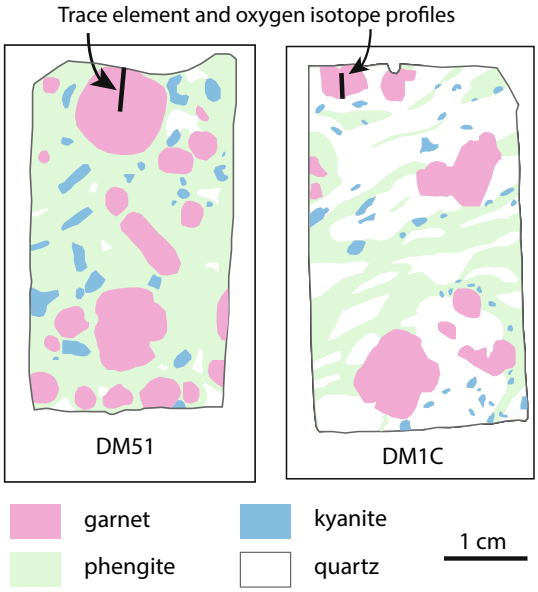

Fig. 1 Schematic drawing of major phases in DM1C and DM51 thin sections. Retrogression coronas have been integrated into the area allocated to garnet in order to reconstruct the peak metamorphic modal composition

Garnets from sample DM1C (5 mm in diameter) display a regular bell-shaped decrease in Fe and Mn from core to rim resulting in an increase in the pyrope content from 85 to 99 %. Grossular contents are below 3 % (Online Resource 1, Online Resource 2). Chondrite normalised patterns (Fig. 2, Online Resource 1) show strong core–rim variations within garnet, from a LREE-depleted and flat HREE to a pattern characterised by a steep decrease in HREE after a peak at Gd–Tb. A small negative Eu anomaly is present throughout the garnets, and HREE and Y are gradually depleted from core to rim in both samples. The strong variation in HREE and the presence of high Y and HREE cores indicate that equatorial sections through the garnets were likely analysed.

Samples DM51–53 have been collected in the inner part of the whiteschist lens in horizons that are characterised by abundant garnet (up to 10 cm in size). Garnet is embedded in a kyanite-bearing phengite matrix, where quartz is a

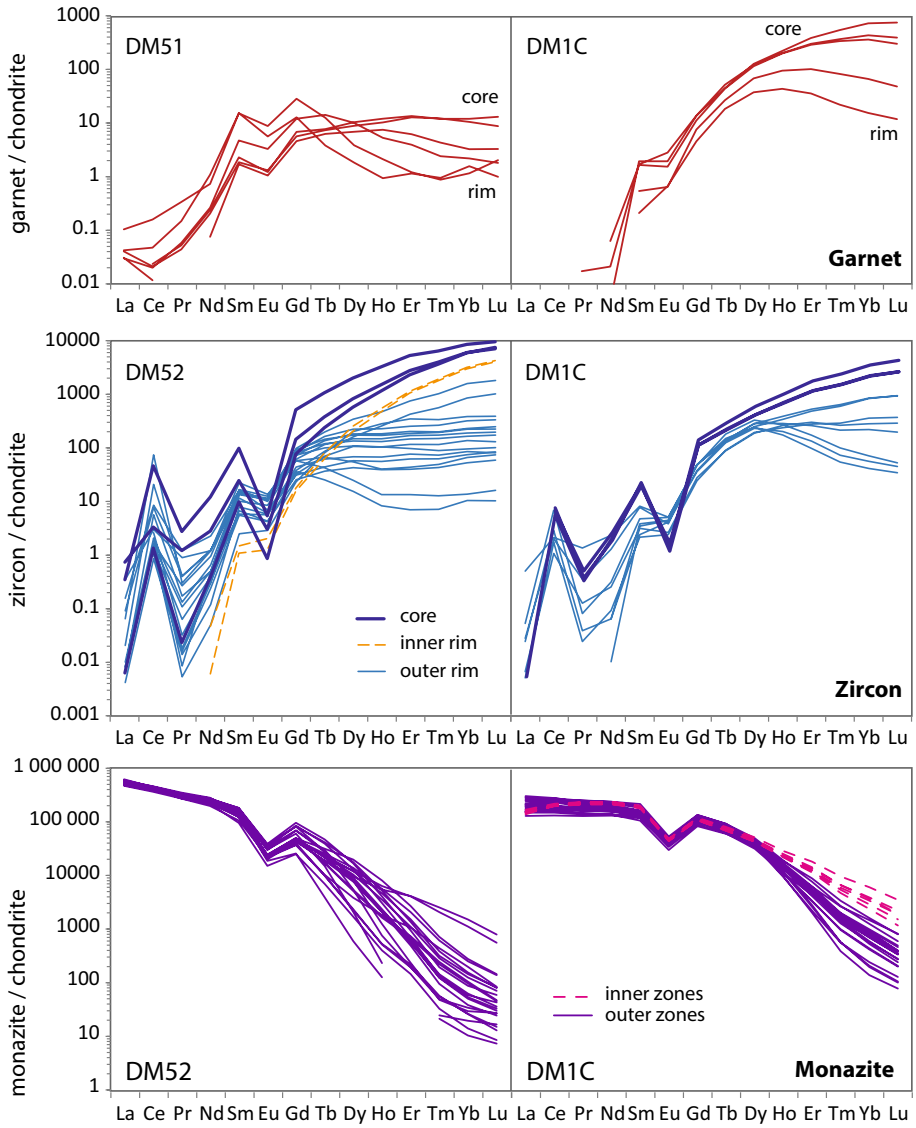

Fig. 2 REE patterns normalised to chondrite (Sun and McDonough 1989) for representative garnets, zircon and monazite from SiO_2-rich (DM1C) and SiO_2-poor samples (DM51–53)

minor phase (Fig. 1). Rutile occurs as inclusions in garnet as well as in the matrix. Bearthite can be found as inclusions in garnets. Many of the large garnets contain inclusions of quartz after coesite that are surrounded by radial cracks. On mineral separation, abundant zircon and monazite were retrieved. These samples display a higher degree of retrogression with talc + kyanite replacing pyrope garnet.

Garnets in DM51 are up to 1 cm in diameter and display a less pronounced variation in pyrope content from Py_{96} in the centre to Py_{99} in the rim. Trace elements in garnets have been analysed as spot analyses along a traverse from core to rim (Fig. 2, Online Resource 1). The HREE patterns in the cores are flat at about 10 times chondrite and their abundance decreases towards the rims, whereas the MREE contents increase slightly. The relatively high pyrope content and the lack of a pronounced enrichment in Y and HREE suggest that the section did not go through the exact core of the garnet.

Zircon textures, inclusions and composition

Zircons in all samples are either rounded and translucent or more elongated and slightly pink in colour. Their size ranges from 20 to 300 µm in length. In CL, they show oscillatory-zoned cores and 1 or 2 unzoned rims that have distinct CL emission (Fig. 3a). The cores are dusted with fluid and mineral inclusions and show embayments and resorption features. In the quartz-poor samples DM51–53, the core is directly overgrown by a CL-bright inner rim that rarely exceeds a few microns in thickness. In these samples, an outer zircon rim, which is darker in CL and shows weak zoning, is present in most crystals. In sample DM1C, the oscillatory-zoned

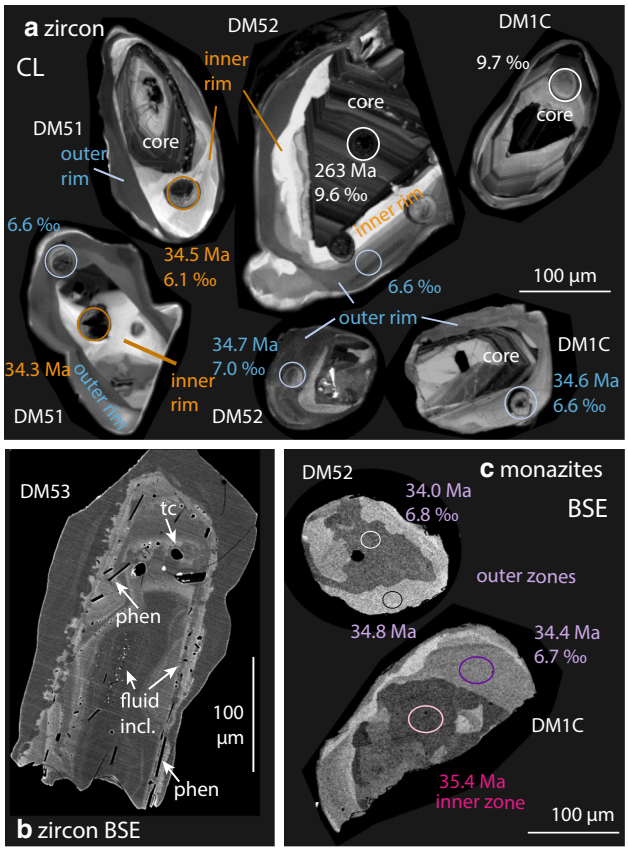

Fig. 3 CL and BSE images of zircons and monazites. Ages and $\delta^{18}O$ values were obtained by SHRIMP analyses on two successive polished surfaces

zircon cores are overgrown by a single rim that is free of inclusions.

In all samples, oscillatory-zoned cores have a steep HREE pattern, with a pronounced negative Eu anomaly (Eu/Eu* 0.02–0.06, Fig. 2, Online Resource 3). The inner zircon rims in sample DM52, DM51 and DM53 yield steeper patterns that are HREE-rich and slightly MREE-depleted with respect to the cores (DM52 where more analyses could be performed is shown in Fig. 2). The outer rims in all samples are gradually depleted in HREE compared with the oscillatory-zoned cores and DM51, DM52 and DM53 inner rims. All rims display a weak negative Eu anomaly (Eu/Eu* 0.15–0.30) and a positive Ce anomaly. Outer zircon rims are depleted in MREE compared to the cores, a depletion that is not observed in DM1C zircons where Dy contents are similar in cores and rims.

DM1C zircons contain inclusions of phengite, talc, florencite, monazite, phlogopite and apatite. In sample DM52–53, zircons contain phlogopite, chlorite, phengite, monazite, bearthite and apatite. Inclusions are only present within the oscillatory-zoned cores of the investigated grains, most concentrated in oscillatory bands that are

Table 1 EDS chemical composition of mineral inclusions in DM52 zircons

Mineral	Phl	Phl	Phe
wt%			
SiO_2	45.7	42.4	53.7
TiO_2	0.4	0.3	0.3
Al_2O_3	13.0	16.1	23.1
FeO	0.3	0.5	0.1
MgO	24.7	23.8	6.2
Na_2O	0.1	0.2	0.2
K_2O	8.6	9.3	9.9
ZrO_2	0.2	0.1	0.2
Total	93.0	92.6	93.7
Si	3.19	3.00	3.59
Ti	0.02	0.02	0.02
Al	1.07	1.34	1.82
Fe^{2+}	0.02	0.03	0.00
Mg	2.57	2.51	0.62
Na	0.02	0.03	0.02
K	0.76	0.84	0.85
X_{Mg}	0.99	0.99	1.00

Cation proportions are calculated for 11 oxygens (phengite) and 11 oxygens (phlogopite)

lighter in BSE (U-rich domains), as well as the interface between core and inner rim (Fig. 3b). Phengite and phlogopite inclusions away from cracks yield high Si content (between 3.5 and 3.6 Si pfu in phengite; 3.0 and 3.2 Si pfu in phlogopite, for analyses that show no detectable contamination from the host zircon, Table 1). Micron-sized, round fluid inclusions are present together with the mineral inclusions (Fig. 3b). On polished surfaces, these inclusions appear only partly filled and EDS analyses show variable amounts of Na, Al, Cl, K Ca and likely Si (which is more difficult to detect due to overlap with zircon).

Monazite textures and composition

Samples DM51–53 contain abundant monazite grains that are yellow to green in colour and range in size from 100 to 200 µm. In these samples, monazite contains moderate amounts of Th (up to 12 wt%, Online Resource 4). In Si-rich sample DM1C, monazite grains are rare, green in colour and with higher U and Th contents (up to 5 and 30 wt%, respectively) incorporated mainly by cheralite [CaTh$(PO_4)_2$] substitution. Monazite zoning in BSE images (Fig. 3c) displays both banded and patchy zoning, but these domains are not organised in a systematic core–rim structure. Microprobe analysis shows that BSE brightness is correlated to Th content. Monazites yield a steep pattern, LREE-rich pattern with a gradual HREE depletion in the

outer zones (Fig. 2). In sample DM52, MREE are depleted in the HREE-poor zones compared with the HREE-rich zones, whereas in DM1C, as for zircon, the Dy content is similar in inner zones and outer zones. A weak negative anomaly in Eu is observed in all analyses.

Thermodynamic modelling of Si-poor whiteschists

The metamorphic reactions resulting in fluid liberation during prograde subduction are different for Si-rich and Si-poor (chlorite-rich) whiteschists (Hermann 2003).

Si-rich whiteschists

Experiments have shown that in Si-rich whiteschists similar to DM1C, chlorite is completely consumed when it reacts with quartz to produce kyanite and talc on the prograde path through the univariant reaction in MASH:

$$\text{Chlorite} + \text{Quartz} \rightarrow \text{Talc} + \text{Kyanite} + \text{aqueous fluid} \quad (1)$$

Garnet formation in the pure MASH system is restricted to UHP conditions and forms at ~40 kbar, 720 °C through the univariant reaction:

$$\text{Kyanite} + \text{Talc} \rightarrow \text{Garnet} + \text{Coesite} + \text{aqueous fluid} \quad (2)$$

A pseudosection was produced for Si-rich whiteschist DM1C (Online Resource 5), to complement the experimental work by Hermann (2003) in the KMASH system. The bulk rock composition was calculated from mineral modes observed in thin section (phengite 30 %, garnet 18 %, kyanite 3 % and coesite 49 %, Fig. 1). A pure pyrope garnet and the phengite composition measured in DM1C by Hermann (2003) were used. The Fe content was then calculated using the bulk rock Mg content obtained from the thin section minerals modes and published bulk rock Mg# of 0.8, which is fairly constant in different whiteschists (Ferrando et al. 2009). The resulting bulk rock is 76 wt% SiO_2, 13 wt% Al_2O_3, 1.75 wt% FeO, 7 wt% MgO and 3 wt% K_2O. H_2O was assumed in excess and all Fe was considered Fe^{2+}. The thermodynamic calculations are done using the programs Theriak and Domino (de Capitani and Petrakakis 2010), using the tcdb55c2d database (Holland and Powell 1998) with default solution models (white mica: updated tc325, Coggon and Holland 2002, garnet and biotite: tc330 based on White et al. 2007, orthopyroxene: tc330 based on White et al. 2002, 2007).

Most of the water (3.2 vol %) is released by the chlorite breakdown reaction (1). The addition of Fe transforms the univariant reaction into a continuous reaction with formation of kyanite at 17 and chlorite disappearance at 19 kbar for the chosen subduction trajectory. No biotite is stabilised on the prograde path. The addition of Fe results in very small amounts of garnet being formed already at 20 kbar. Also the univariant reaction (2) in MASH transforms into a continuous reaction in FMASH with most of the garnet (9 vol % of the 17 vol %) and the water (1.1 of 1.9 vol %) produced between 35 and 38 kbar (Online Resource 6). Thin section observations and chemical analyses have shown that garnets have Fe enriched in the core. To evaluate the effect of this Fe sequestration, we have also calculated a Fe-free pseudosection (Online resource 7). The main difference is that the now univariant reaction (1) is shifted up temperature by about 20 °C and up pressure of about 2 kbar for the given subduction trajectory and the fluid release will be in a sharp pulse. Garnet rims have Py_{99} and form at ~730 °C, 40 kbar.

Si-poor whiteschists

DM51–53 belong to the Si-poor type of Hermann (2003), and in these rocks, chlorite is in excess and quartz reacts out during prograde metamorphism (reaction 1). With chlorite persisting to higher pressures, there is the possibility for additional dehydration reactions during the prograde path. In order to investigate the fluid release in these Si-poor whiteschists, we have calculated a pseudosection for sample DM51 in KFMASH. The bulk composition calculated in the same way as DM1C is 53 wt% SiO_2, 26 wt% Al_2O_3, 3.5 wt% FeO, 14 wt% MgO and 6.6 wt% K_2O.

The calculated pseudosection for the Si-poor whiteschist DM51 is given in Online Resource 8. As we are most interested in the release of fluid during prograde metamorphism, we have calculated the relative phase abundances along a path from 600 °C, 15 kbar to 720 °C, 42 kbar in 200 steps using the program Theriak (Fig. 4a). The modelling shows that a first pulse of fluid production (0.4 % of rock volume, Fig. 4b) occurs at around 17 kbar when quartz disappears in reaction with chlorite to produce kyanite and talc. Shortly after, a small amount of garnet starts growing at the expense of chlorite, resulting in a gradual release of water by the reaction:

$$\text{Chlorite} + \text{Kyanite} + \text{Talc} \rightarrow \text{Garnet} + \text{aqueous fluid} \quad (3)$$

The most significant fluid pulse with 3.4 vol % water released is when chlorite disappears along the reaction at 22 kbar and biotite with a phlogopite composition is produced:

$$\text{Chlorite} + \text{Phengite} \rightarrow \text{Kyanite} + \text{Biotite} + \text{aqueous fluid} \quad (4)$$

It is worth noting that in Si-rich whiteschists, no biotite appears on the prograde path. In the Si-poor samples, biotite then is consumed along the continuous reaction to form more garnet and liberating additional aqueous fluid

$$\text{Biotite} + \text{Kyanite} + \text{Talc} \rightarrow \text{Garnet} + \text{Phengite} + \text{aqueous fluid} \quad (5)$$

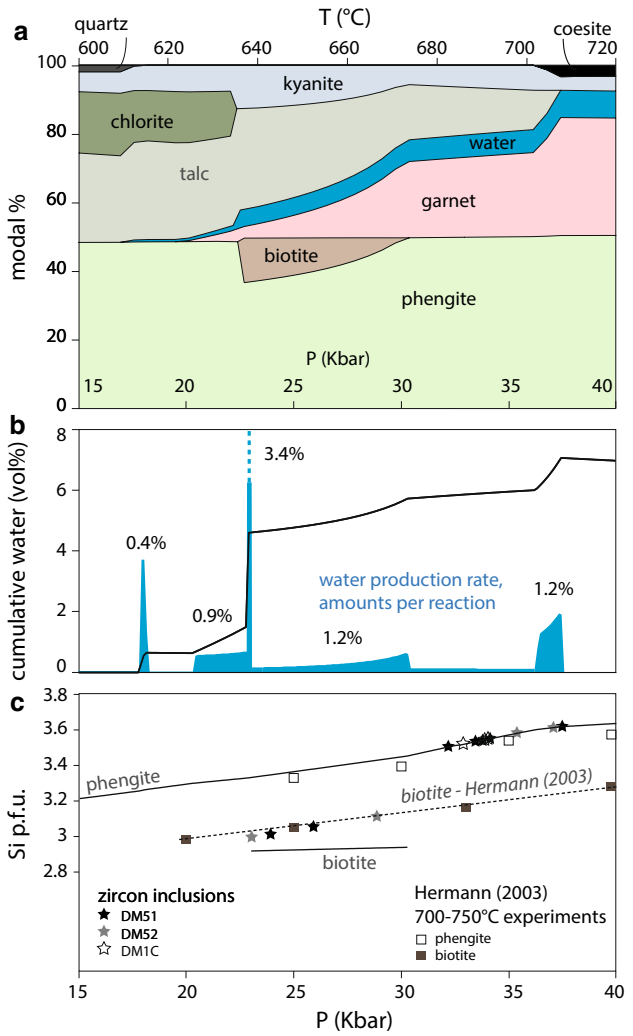

Fig. 4 Theriak modelling results along a P–T path from 15 kbar, 600 °C to 40 kbar, 720 °C for Si-poor sample DM51. **a** Volume % of mineral phases. **b** Cumulative water release and rates of release (qualitative only) with total volume % of water released per reaction. **c** Si per formula unit in phengite as predicted by the Theriak model (Holland and Powell database, *continuous lines*), and biotite from Hermann (2003) experiments (*dotted line* and *squares*) compared to measured values in zircon inclusions (*stars*, typical precision is within the height of the symbol)

A third pulse of fluid liberation occurs at the final consumption of talc at the same reaction that also produces garnet in the Si-rich whiteschists (1).

Similarly to the Si-poor composition, Fe in DM51 composition increases the stability fields of garnet and chlorite, shifting reaction (1) to lower P and T, and reactions (5) and (2) to higher P and T (see Fe-free pseudosection in Online Resource 9). As for DM1C, fractionation of small volume of garnet after reaction (3) will inhibit further prograde garnet growth and shift the biotite breakdown (5) and talc breakdown (2) to higher P and T. The position of reaction (1) should be accurate as the Fe will be available for reaction in chlorite, and the position of the reaction (4) is not affected significantly. In terms of fluid production, the main difference is that the third fluid pulse is shifted up in temperatures by about 20 °C along the chosen subduction geotherm and that the fluid will be released over a smaller temperature interval.

U–Pb dating

Most analysed oscillatory-zoned zircon cores have small amounts of common Pb (common ^{206}Pb up to 1.7 %); they are discordant and scatter in apparent age from ca. 270 to ca. 100 Ma. The four oldest dates in DM52 are concordant with an average ^{206}Pb/^{238}U age of 261 ± 9 Ma (Fig. 5, Online Resource 10). The zircon cores contain between 800 and 2000 ppm U and have a relatively high Th/U of 0.2–0.5. Inner zircon rims in DM52 are moderately U-rich (300–700 ppm) and are Th-poor with a Th/U of 0.01. Only a few analyses could be placed on this thin inner rim, and their average age is 35.1 ± 0.5 Ma (n = 3, Figs. 5, 6). In DM51, inner zircon rims are broader and more could be analysed; they yield a similar age of 34.5 ± 0.7 Ma (n = 6). U content of the inner zircon rim is between 200 and 300 ppm, and Th/U is low at 0.13–0.05. Outer zircon rims are abundant in sample DM52, are rich in U (300–1700 ppm, Th/U of 0.01–0.05) and yield an age of 34.9 ± 0.2 Ma (n = 13). A rim age of 35.1 ± 0.8 Ma (n = 5) is obtained for DM1C zircons, which are relatively poor in U (56–580 ppm, Th/U 0.10–0.01).

Most of the monazite analyses in the Si-poor samples DM51 and DM52 yield an unusually high proportion of initial lead (from 11 % to 80 % ^{206}Pb, Online Resource 11), for U contents between 50 ppm and 1 wt%. DM1C monazites are particularly Th and U-rich up to 30 and 5 wt%, respectively, and contain significant amounts of initial ^{206}Pb (1–10 %). In either samples, defining the composition of the initial lead is crucial to accurately determine the age of the monazites. Uncorrected data plotted in Tera–Wasserburg diagrams (Fig. 5) define a linear regression whose upper intercept indicates a ^{207}Pb/^{206}Pb composition of initial Pb that is best determined in DM52 at 0.7154 ± 0.017 (MSWD = 1.5). In the two other samples, the regression is poor and the obtained initial lead composition is not robust (0.750 ± 0.039, MSWD = 4.5 for DM51 and 0.652 ± 0.063, MSWD = 2.3, for DM1C). The values for all three samples are lower than the model common ^{207}Pb/^{206}Pb ratio of 0.838 at 35 Ma according to Stacey and Kramers (1975). This indicates that the initial lead present in the monazites has a radiogenic component. Identical free intercept ages are calculated for the two samples where the regression is better defined: DM52 yields an age of 33.8 ± 0.9 Ma (MSWD = 1.5) and DM1C an age of 33.8 ± 0.7 Ma (MSWD = 2.3). Monazite analyses in

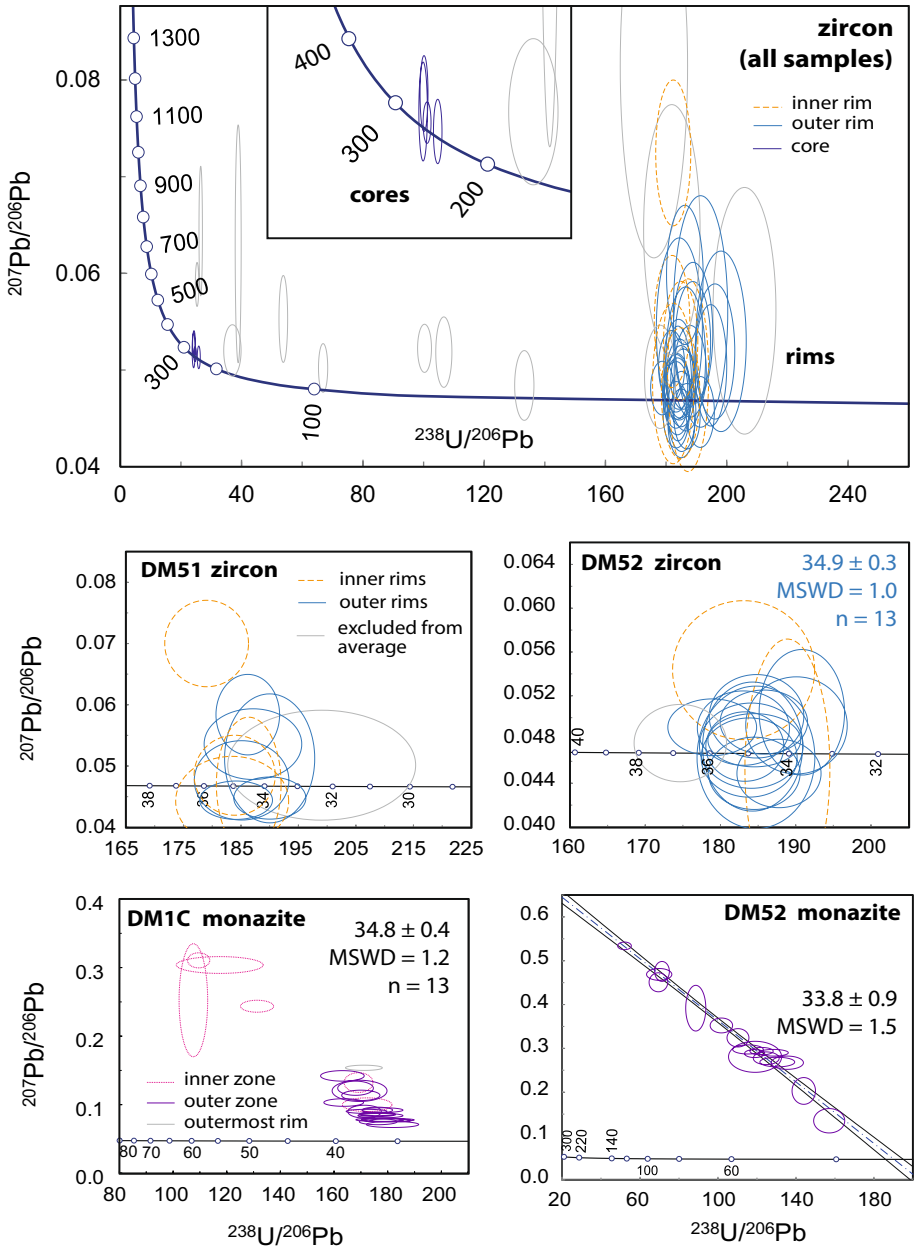

Fig. 5 Tera–Wasserburg diagrams for U–Pb analyses of zircon and monazite, uncorrected for initial Pb

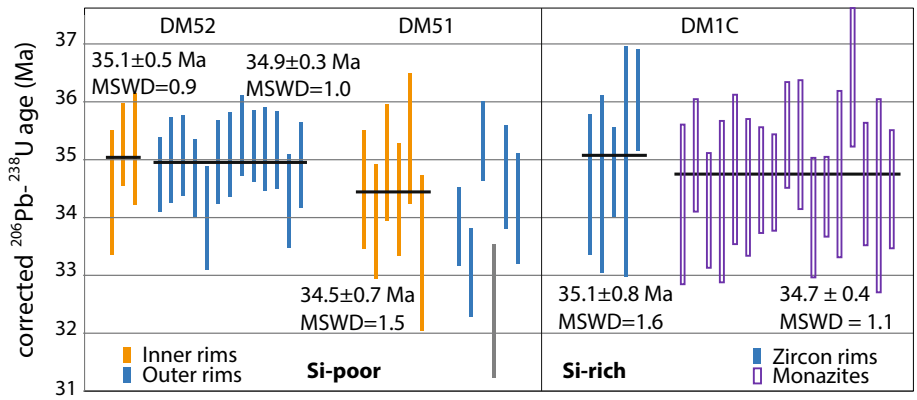

Fig. 6 Summary of ^{206}Pb–^{238}U ages for zircon and monazite corrected for initial Pb

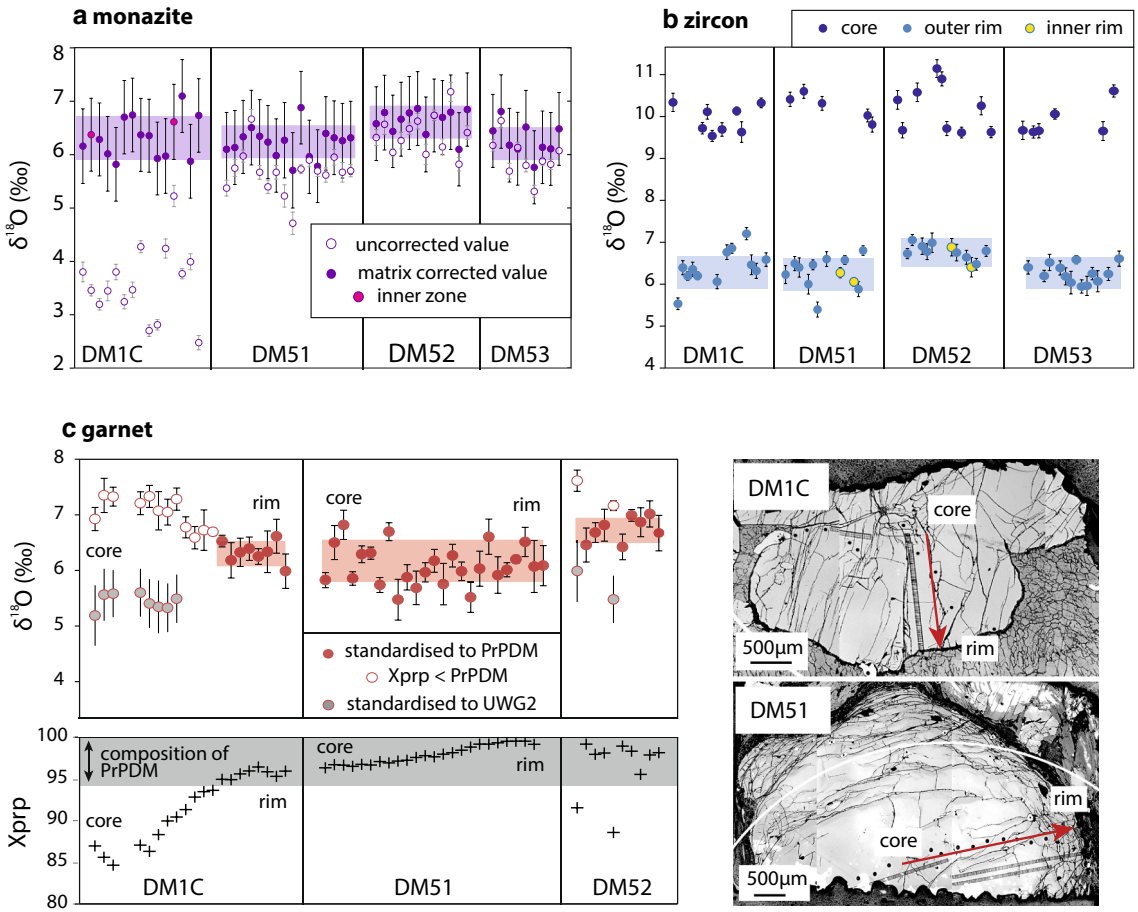

Fig. 7 Oxygen isotope analyses in monazite, zircon and garnet. Reflected light images of the analysed garnet grains are presented on the *bottom right panel*. Individual *error bars* represent 2SE for uncorrected measurements only; for corrected measurements (monazite and garnet), the uncertainty includes SE on the measurement, SE from the matrix correction residual and SE for the reference value of the standard (as per Martin et al. 2014; Rubatto et al. 2014). In **a**, the values corrected for matrix effect (see text for details) are plotted together with the uncorrected values. Garnet measurements were generally standardised to PrPDM pyrope standard, but for garnet with pyrope content below 95 % standardisation to UWG2 garnet was preferred (see text for details)

sample DM51 are more scattered and contain the largest initial lead contribution. A poorly defined regression gives an age of 36.8 ± 3.5 Ma with a high MSWD of 4.5. Seventeen analyses of DM1C monazite contain less than 10 % initial Pb, and when the intercept is forced to the model common Pb composition (Stacey and Kramers 1975), they yield a weighted average $^{206}Pb/^{238}U$ age of 34.7 ± 0.4 Ma which is within the error of the intercept age for the same sample.

It has been previously reported that the preferential incorporation of Th relative to U in minerals such as monazite from a short-lived melt or fluid can induce a disequilibrium in the Th–U series: namely, excess ^{230}Th incorporated at the time of monazite crystallisation can lead to the production of excess ^{206}Pb. This effect can be estimated in magmatic systems (Schärer 1984), but it is hard to assess whether monazite crystallises from an aqueous fluid as the fluid Th/U is unknown. If corrected on the basis of the measured ^{204}Pb and a Stacey and Kramers (1975) common Pb composition, all but three Pb-rich analyses in DM1C are concordant in the conventional Wetherill diagram and give a weighted average of 34.6 ± 0.3 Ma. Excess ^{206}Pb would affect only one of the two decay systems, thus concordance is taken as evidence that any potential ^{206}Pb excess is within the analytical error of the analyses in these monazites. In other samples, excess ^{206}Pb is also expected to be within analytical uncertainty even though the amount of initial Pb prevents performing the same test.

SHRIMP oxygen isotopes

Oxygen isotopes in zircon were measured on the same domains as U–Pb ages. Across individual samples, oscillatory-zoned zircon cores yield $\delta^{18}O$ average values between 9.9 ± 0.4 and 10.2 ± 0.4 ‰, 2σ (Fig. 7b, Online Resource 12). The scatter observed in samples DM52 and DM53 is

slightly larger than that measured for Temora standard, and it is speculated that this may be the effect of the micro-inclusions visible in this domain. This is supported by the metamict aspect of the zircons cores and their discordant U–Pb dates.

Zircon rims yield $\delta^{18}O$ average values between 6.2 ± 0.4 ‰ in DM53 and 6.7 ± 0.4 ‰ in DM52 for about 10 analyses in each sample (Fig. 7b). A few inner rims were analysed in sample DM51–53 and yield the same $\delta^{18}O$ value of around 6.4 ‰. Some scatter is present in zircon analyses from DM1C and DM51, and this is attributed to small amounts of mixing between core and rim or with inclusions.

Core–rim profiles for $\delta^{18}O$ have been measured in one DM1C and one DM51 garnet along the same direction of the trace element profiles and in DM52 garnet fragments. Using pyrope PrPDM (Vielzeuf et al. 2005; Page et al. 2010) as a matrix-matched primary standard, the averages $\delta^{18}O$ values measured for pyropes (X_{Pyr} 0.95–0.99) are between 6.3 ± 0.2 ‰ and 6.8 ± 0.3 ‰ (Fig. 7c, Online Resource 2). For these compositions, the value obtained in the garnet core is indistinguishable from the rim. DM1C garnet core lies outside of the compositional range matched by PrPDM, with X_{Alm} as high as 0.11. This results in higher measured apparent values (up to 7.4 ‰) against PrPDM. This is believed to be the effect of a Mg#-related matrix effect at high X_{Prp} that has not been previously described, as these compositions were not covered by Martin et al. (2014). Indeed, analysing pyrope garnet PrpDM using UWG2 (Valley et al. 1995, X_{Grs} 0.14, X_{Pyr} 0.40 X_{Alm} 0.45) as primary standard and applying the Martin et al. (2014) correction for the grossular component of the garnet, the $\delta^{18}O$ value obtained for PrPDM ($0.95 < X_{Pyr} < 0.99$) is 4.2 ‰, instead of the published value of 5.6 ‰ (Vielzeuf et al. 2005). This test implies an additional matrix bias of −1.4 ‰ for near-endmember pyropes compared to the calibration of Martin et al. (2014). Therefore, in order to get a lower bracketing value, DM1C cores with $X_{Pyr} < 0.90$ were standardised to UWG2 and corrected for their grossular component according to Martin et al. (2014); this yielded a $\delta^{18}O$ value of around 5.6 ‰ (Fig. 7c). The true value of these cores is believed to lie between 7.4 and 5.6 ‰ (standardised to PrPDM and UWG2 with correction, respectively).

In monazites, analyses corrected for the huttonite and cheralite component (see details in Rubatto et al. 2014) for DM51, DM52 and DM53 yield homogenous populations with $\delta^{18}O$ of 6.4 ± 0.7, 6.8 ± 0.7 and 6.6 ± 0.7 ‰, respectively (Fig. 7a, Online Resource 13). For the cheralite-rich DM1C monazites, the average $\delta^{18}O$ is 6.3 ± 0.8 ‰. Monazites in all samples are homogenous and identical within uncertainty in their oxygen isotopic composition.

Discussion

We will first assess the conditions of metamorphic zircon and monazite growth and link this to fluid release in the whiteschists, to constrain the mechanisms of formation/recrystallisation of these accessory phases. This provides the basis for the interpretation of the dating results, that are used to estimate subduction rates. The addition of in situ oxygen isotope measurements in garnet, monazite and zircon provides a framework to trace fluid–rock interactions from the intrusion of Permian granites to Alpine UHP metamorphism.

Metamorphic conditions of zircon and monazite growth

The first step for the interpretation of the obtained ages and in situ oxygen isotope data is the correlation of zircon and monazite domains to metamorphic conditions. The garnet-forming reactions in Si-rich and Si-poor whiteschists are well constrained by experimental results (Hermann 2003) and thermodynamic modelling (Figs. 4 and 8, Online Resource 4). The relative growth of zircon and monazite domains with respect to garnet can be assessed based on REE patterns (e.g. Rubatto 2002). Garnets from samples DM1C and DM51 show a gradual depletion in Y and HREE from core to rim. Preserved small-scale variations indicate that diffusion is not significant for trace elements at these temperatures, as shown by previous studies (e.g. Hermann and Rubatto 2003). With enrichments up to 1000 chondrite in Lu and modal abundance between 20 and 40 %, garnet is the main host for HREE in all analysed whiteschists. The HREE depletion is thus interpreted as growth zoning, reflecting Raleigh fractionation (Otamendi et al. 2002) of REE and Y. This effect is much more pronounced in whiteschist DM51 where the garnets are larger and more abundant. It is likely that our profile in DM51 garnet is not exactly equatorial and does not include the true core compositions. Garnet REE patterns also show a small negative Eu anomaly that is unchanged from core to rim and is comparable in magnitude to that of the bulk rock (Grevel et al. 2009). This suggests that no other phase capable of fractionating Eu, such as plagioclase, was present in the metamorphic assemblage throughout garnet growth.

The second zircon rim in samples DM51–53 and the rim overgrowing the cores in DM1C zircons yield variable depletion in HREE and Y of the same magnitude as observed in garnet, as well as a weak negative Eu anomaly. Using analyses from sample DM1C, calculated zircon–garnet HREE partitioning between garnet and zircon rims is between 17–20 for Lu, down to 4–7 for Er. This is comparable to previous coefficients determined in experimental and natural samples at similar temperatures (600–800 °C;

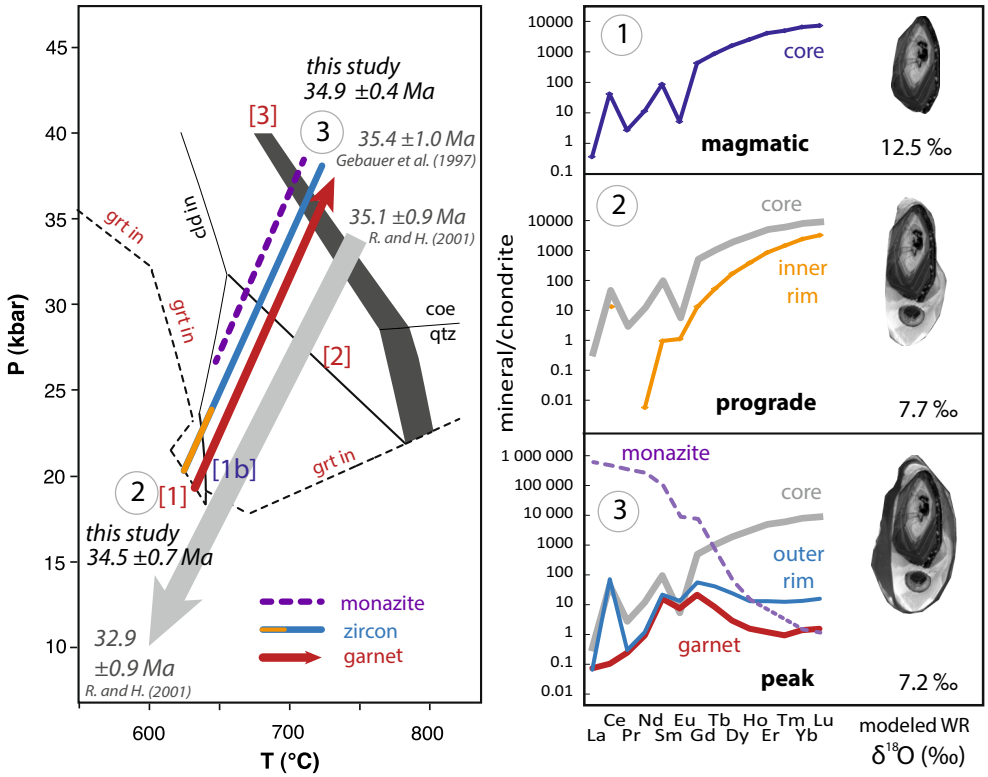

Fig. 8 Summary of P–T–time path (*left*) and zircon record (*right*). Garnet-forming reactions reported in the P–T path are from our modelling (Online resource 4) *1* chl + ky + tc → grt + liq, *2* bt + ky + tc → grt + phe + liq, *3* ky + tc → grt + coe + liq. Main dehydration reaction *1b* chl + phe → bt + ky + liq. Exhumation path (*thick grey arrow*) is from Rubatto and Hermann (2001). Ages are from DM51 zircon inner rims (*2*) and DM1C zircons rims (*3*). For the three major stages, magmatic, prograde and peak, we report on the right the REE patterns from DM52 zircon and monazite, and DM51 garnet, as well as a modified CL image of a representative zircon from DM51. The modelled whole-rock (WR) oxygen estimates are based on the average zircon core $\delta^{18}O$ (magmatic stage) and the DM51, 52, 53 inner and outer zircon rim averages (prograde and peak stage, respectively)

Rubatto 2002; Rubatto and Hermann 2007) and might be taken as an indication for equilibrium between zircon and garnet. Because these garnets have a different composition to the experiments and natural samples considered by previous studies, the comparison of partitioning values is indicative only. On the basis of their trace element composition relative to garnet, the outer zircon rims are interpreted as crystallising during the growth of HREE-depleted garnet. These rims yield an average age of 34.5 ± 0.4 Ma in quartz-poor, garnet-rich samples DM51 and DM52, which is interpreted as the average age of peak garnet growth along reaction (2). In the quartz-rich sample DM1C, where garnet grows close to peak conditions (Hermann 2003, this study, Prp II in Ferrando et al. 2009), zircon outer rims yield scattered analyses around the same age (Fig. 5).

In samples DM51–53, the inner zircon rim directly overgrowing the cores is distinct in chemistry with a low U content, steep HREE patterns (similar to the cores, but distinct from the other rims) and small negative Eu anomaly that is of the same magnitude as the bulk rock, but weaker than the zircon cores. These features suggest that the inner zircon rim grew in the absence of significant modal garnet and plagioclase (Rubatto 2002). We interpret these observations as first growth of zircon during prograde metamorphism, before significant garnet growth. According to our thermodynamic modelling, garnet growth in these Si-poor whiteschists starts already at ~22 kbar, along the reaction (3) described first in Chopin (1984) and further in Schertl et al. (1991), and thus, the inner zircon rim likely formed close to this pressure. This first growth of pyrope corresponds to Prp I in Ferrando et al. 2009.

Mineral inclusions provide additional information on the growth of the metamorphic zircon domains. The interpretation of these inclusions is complicated by the fact that most inclusions occur in the zircon cores (see next section). The inclusions are small (a few microns) and thus difficult to analyse, but some important inferences can still be made from their mineralogy and composition. Zircons from Si-rich and Si-poor whiteschists contain abundant talc and phengite inclusions, indicating that these inclusions were captured when talc was still a stable phase. The Si pfu of most of the included phengites is around 3.5, and only few

phengites show a Si pfu of 3.6 that is comparable to the peak phengite in the matrix. According to the experiments and thermodynamic calculations (Fig. 4a, c), phengite with 3.5 Si pfu and talc coexist just before the final breakdown of talk. Combined with the REE characteristics, the inclusions thus provide evidence that the outer zircon rims formed at the talc-out and garnet-forming reaction (2) on the prograde path at 700–720 °C, 35–40 kbar. In the Si-poor whiteschists, zircon hosts phengite with a lower Si content and phlogopite. The presence of phlogopite is very important as it occurs only in a restricted P–T interval on the prograde path. The thermodynamic model does not include a biotite solid solution that permits Si > 3 pfu. However, in the experiments of Hermann (2003), changing phlogopite compositions with pressure are reported and these can be used to constrain the pressure of trapping of the phlogopites to 22–25 kbar. This pressure estimates coincide with the calculated stability field of biotite (Fig. 4a, Online Resource 4). Together with the HREE-enriched characteristics of the inner zircon rim, these inclusions suggest that the inner metamorphic rim found in the zircons of Si-poor whiteschists formed at ~22 kbar, 640 °C.

In all samples, prograde phosphate phases such as bearthite, florencite or apatite, as well as monazite are found as inclusions in zircon. This indicates that the transition of prograde phosphates to monazite occurred within the P–T range at which zircons recrystallised, potentially at the time of Prp I growth in DM51 or the main garnet growth (Prp II in Ferrando et al. 2009) event in DM1C. Monazite records a similar chemical evolution as observed in garnet and zircon (Fig. 2). Monazite in Si-poor samples DM51–53 as well as the outer monazite growth zones in DM1C shows HREE and Y depletion and a weak negative Eu anomaly. Based on the REE record, monazite is interpreted to recrystallise during the main prograde episode of garnet growth (22–40 kbar). Monazite yields Alpine ages that are best determined for sample DM1C (34.7 ± 0.5 Ma). We conclude that monazite grew during prograde to peak Alpine metamorphism together with garnet and zircon outer rims.

Fluid-induced prograde zircon formation

The correlation of zircon formation to metamorphic conditions revealed that two distinct episodes of zircon recrystallisation coincide with the major dehydration reactions. In Si-rich whiteschists, chlorite disappears between 17–19 kbar and 610–620 °C when chlorite + quartz react to form talc + kyanite plus an aqueous fluid. The second fluid-producing reaction occurs close to peak pressure where talc + kyanite react to form garnet + coesite. Zircons retrieved from such Si-rich whiteschists display only one metamorphic overgrowth. Inclusion compositions as well as REE patterns suggest rim formation close to peak metamorphic conditions, when most of the garnet grew. Zircons from Si-poor whiteschists present an additional inner rim that likely formed during the complete consumption of chlorite, representing the main fluid pulse in these rock types (Fig. 4b). The fluid liberation event from the destabilisation of chlorite at 640 °C and 22 kbar could correspond to the first generation of fluid inclusions (a NaCl–$MgCl_2$–rich brine) described by Ferrando et al. (2009) during the initial growth of pyrope (Prp I in Ferrando et al. 2009). The destabilisation of biotite and talc at 29–37 kbar also produced fluids that would correspond to a more solute-rich composition of potentially supercritical character, containing Al, Si, Mg and a range of trace elements (Philippot et al. 1995; Ferrando et al. 2009), during the growth of Prp II and Prp III.

The distribution of inclusions in the zircons provides additional clues on the mechanisms of zircon formation during prograde fluid liberation. The great majority of inclusions are hosted within the inherited zircon cores. The magmatic zircon cores show signs of partial dissolution: the oscillatory zones are truncated, show embayments and are peppered with mineral and fluid inclusions. In DM51 and DM52, these inclusions contain talk, phengite and phlogopite whose chemistry is similar to what was experimentally obtained by Hermann (2003) for prograde to peak phengite and prograde phlogopite (Fig. 4c). These results complement a study by Schertl and Schreyer (1996) where they found prograde phases such as talc and chlorite in crushed zircon separates along with coesite and phengite with 3.50–3.55 Si pfu. These authors also found a single inclusion of pyrope that yielded the same composition as the core of the groundmass pyropes in the same sample. Schertl and Schreyer (1996) noted that most inclusions occurred in the central part of the zircon grains and in the absence of in situ dating work concluded that they were primary inclusions in metamorphic zircon crystals. By imaging, dating and measuring the composition of the inclusions in situ, we are able to determine that they are in fact secondary inclusions (as mentioned in Gebauer et al. 1997 on the basis of CL images), crystallising during partial dissolution of the magmatic cores during Alpine HP to UHP metamorphism. A similar case was documented for zircon within an UHP gneiss recovered from the deep Chinese Continental Scientific Drilling project, where coesite and jadeite were found within partially altered inherited cores (Zhang et al. 2009). Interestingly, the metamorphic inclusions in zircons from the whiteschists are more abundant in the BSE-light, U-rich oscillatory zones (Fig. 3b) which may have been selectively dissolved due to radiation damage and metamictisation. All these observations suggest that the main process for new zircon growth in the Dora-Maira whiteschists is related to fluid-induced dissolution–precipitation during metamorphism as previously described in other high-pressure

Table 2 Sample average $\delta^{18}O$ and calculated fractionation values between zircon, monazite and garnet

Sample	Zircon rims		Monazites		Garnet		Zircon–monazite		Zircon–garnet	
	$\delta^{18}O$ ‰	2se	$\delta^{18}O$ ‰	2se	$\delta^{18}O$ ‰	2se	$\Delta^{18}O$ ‰	2se	$\Delta^{18}O$ ‰	2se
DM1C	6.37	0.28	6.34	0.69	6.29	0.29	0.03	0.74	0.08	0.40
DM51	6.35	0.28	6.22	0.69	6.20	0.29	0.13	0.74	0.15	0.40
DM52	6.74	0.29	6.64	0.69	6.86	0.28	0.10	0.75	−0.12	0.40
DM53	6.26	0.29	6.28	0.68	na		−0.02	0.74	na	
					Average	0.06		0.04		

rocks (Tomaschek et al. 2003; Geisler et al. 2007; Rubatto et al. 2008). The type of fluids rich in NaCl and $MgCl_2$ documented in the whiteschists (Philippot et al. 1995; Ferrando et al. 2009) have indeed been shown to enhance zircon dissolution (e.g. Rizvanova et al. 2000). Based on Zr mass balance in metamorphic minerals, Kohn et al. (2015) have suggested that in UHP eclogites, metamorphic zircon should form during the retrograde path rather than during prograde metamorphism. Our study shows that partial dissolution of locally metamict-inherited zircon and precipitation of newly formed zircon rims is a mechanism to form metamorphic zircon on the prograde path, mainly during episodes of intense dehydration or fluid–rock interactions.

Subduction rate

In the previous sections, we have shown that the age of the outer zircon rim (34.4 ± 0.4 and 34.6 ± 0.4 Ma) and that of monazite (34.5 ± 0.5 Ma) dates the breakdown of talc at 35–40 kbar, 700–730 °C. These ages are identical within uncertainty to the titanite age of 35.1 ± 0.9 Ma obtained by Rubatto and Hermann (2001) for peak metamorphism in calc-silicate nodules within the coesite-bearing unit. The ages obtained for the inner zircon rim that likely grew during chlorite breakdown in sample DM51 and DM52 at ~22 kbar, 640 °C are undistinguishable from that of the outer zones. Given that the uncertainty of single analyses is smaller than 0.5 Ma, we can assume that the subduction of the Dora-Maira whiteschists occurred within less than 1–2 million years, for a pressure difference of 13 kbar that correspond to a difference in depth of about 40 km. These values translate into a minimal burial rate of 2 cm/y, which is comparable to exhumation rates calculated for the same unit by Rubatto and Hermann (2001). Our minimum burial rate is close to the Eocene convergence rate of 1.3 cm/y (Ford et al. 2006) along a steep dipping slab as proposed by Carry et al. (2011), although our data allow for an even faster rate. Combining the prograde to peak (this study, Gebauer et al. 1997) and the retrograde ages (Rubatto and Hermann 2001), an exceptionally complete P–T–time path for the subduction and exhumation of this iconic UHP unit can be defined (Fig. 8). Such detail in rates, particularly subduction/burial rates, is hard to obtain because commonly prograde minerals readily recrystallise at the peak or during decompression.

Equilibrium oxygen isotopic fractionation between peak metamorphic phases

Garnet, zircon outer rims and monazites have been shown to crystallise contemporaneously just before peak metamorphic conditions in each individual sample. Their oxygen isotope composition (Table 2) can thus be combined to produce a set of mineral–mineral fractionation values for oxygen. On average $\Delta^{18}O$ (zircon–monazite) obtained from our data is 0.1 ± 0.7 ‰ and $\Delta^{18}O$ (zircon–garnet) is 0.1 ± 0.5 ‰ (Table 2). The temperature at which these minerals formed is estimated to be 680–730 °C (Hermann 2003; this work). The zircon–pyrope results are equal within error to values predicted at 700 °C by previous empirical studies of $\Delta^{18}O$ (zircon–almandine) = −0.07 ‰ (Valley 2003 and references therein) as well as using the increment method (0.0 ‰, Zheng 1993a).

This is the first study looking at zircon–monazite fractionation directly. From previous works, values can be calculated at 700 °C for $\Delta^{18}O$ quartz–zircon (2.41 ‰, Valley 2003; 2.46 ‰, Trail et al. 2009) and quartz–monazite (2.32 ‰, Breecker and Sharp 2007, 1.58 ‰ for Ce–monazite to 2.07 ‰ for huttonite, Rubatto et al. 2014). This set of previous values predicts a $\Delta^{18}O$ (zircon–monazite) at 700 °C from −0.9 to −0.1 ‰: our value of 0.1 ± 0.7 ‰ is consistent with both within error, but agrees best with the quartz–monazite fractionation reported by Breecker and Sharp (2007).

In addition to previous studies, these fractionation values can be used as an additional tool to assess whether accessory phases crystallised in equilibrium with major minerals such as garnet, especially in cases where external fluid influx might lead to a significant change in oxygen isotope values of mineral domains. Any deviation from the described fractionation would indicate disequilibrium due to external fluid influx or temperature changes. Together with trace elements and geochronology at the mineral scale, oxygen isotopic equilibrium between mineral zones can thus be a valid tool to investigate the P–T–time–fluid path of metamorphic rocks.

Table 3 Whole-rock (WR) oxygen isotope modelling from zircon values for Ferrando et al. (2009) DM989, peak conditions DM1C and DM51

Granite DM 989			Whiteschist DM1C			Whiteschist DM51		
CIPW norm ($T = 750$ °C)			Thin section ($T = 720$ °C)			Thin section ($T = 720$ °C)		
Mineral	Mode	$\delta^{18}O$ ‰	Mineral	Mode	$\delta^{18}O$ ‰	Mineral	Mode	$\delta^{18}O$ ‰
Quartz	35	13.1	Quartz	49	9.7	Quartz	3	9.7
Orthoclase	31	12.1	Garnet	18	6.4	Garnet	34	6.4
Albite	23	12.1	Kyanite	3	7.9	Kyanite	7	7.9
			Phengite	30	7.8	Phengite	56	7.8
Zircon	0	10.0	Zircon	0	6.4	Zircon	0	6.4
WR		12.5	WR		8.4	WR		7.4

Evolution of the oxygen isotope composition of the whiteschists from protolith to subduction

The oldest remnants of the evolution of the Dora-Maira whiteschists are preserved in the inherited zircon cores. The least-altered zircon cores display steep REE patterns with enrichment in HREE (Fig. 2) and have a marked negative Eu anomaly (Eu/Eu* 0.02–0.06); this signature is typical of granitic zircons (Hoskin and Schaltegger 2003). The best preserved zircon cores yield Permian ages that are comparable to the ages measured in zircons from the surrounding orthogneiss and other zircon cores in whiteschist analysed by Gebauer et al. (1997). This provides strong evidence that the orthogneiss and whiteschists derived from the same granitic protolith (e.g. Chopin and Schertl 1999). Zircon magmatic cores across the samples yield an average $\delta^{18}O$ of 10 ± 1 ‰. This contrasts with metamorphic zircon domains that yield $\delta^{18}O$ values of 6.4 ‰.

In order to quantify the bulk rock $\delta^{18}O$ change in regard to contributions from temperature, co-crystallising assemblage evolution or metasomatic fluid infiltration, we modelled the $\delta^{18}O$ composition of rock-forming minerals at given temperatures, in equilibrium with the measured zircon values. This is done in a similar way as in Martin et al. (2014): the whole-rock (WR) oxygen is calculated as the sum of the modal contribution of equilibrium fractionation values for minerals. Zircon is present in the model as a spectator phase for which an oxygen value is fixed or calculated but does not participate in the redistribution of oxygen isotopes (its mode is set to 0). The fractionation coefficients between minerals are taken from Zheng (1993a, b) for consistency. Using that set of fractionation coefficients, quartz–water calculations are similar to what is obtained using the most recent Hu and Clayton (2003) experimental coefficients, albeit 0.2 ‰ lower at 600 °C. For other phases, as shown in Kohn (1993), the overall trends obtained for each mineral should not be influenced significantly by the uncertainty related to fractionation coefficients nor small changes in mineral modes.

For the granitic protolith of the whiteschists, the main phases and their modal abundance are calculated from a CIPW norm using the DM989 WR major element analysis from Ferrando et al. (2009). The three major phases quartz, albite and orthoclase are used in the calculation (Table 3). Using the average oxygen value measured in zircon cores (10 ‰), the modelled WR $\delta^{18}O$ of the metagranite is 12.5 ‰ for an estimated magmatic temperature of 750 °C (a higher temperature of 850 °C would shift the value to 12.1 ‰). A calculation based on 73 wt% SiO_2 content following the equation of Lackey et al. (2008) returns a value of 12.0 ‰. This agrees with quartz measurements in the orthogneiss that gave a $\delta^{18}O$ of 11.5–11.9 ‰ (Sharp et al. 1993). Such high values are characteristic of S-type granites that inherit this signature from surface-altered sediments (e.g. Lackey et al. 2008; Jeon et al. 2012).

The peak metamorphic assemblage for the two types of whiteschist DM1C and DM51 is reconstructed using minerals modes from thin section observations (Fig. 1). Using the zircon outer rims values of 6.4 ‰ in both samples, the modelled WR oxygen isotope composition is 8.4 ‰ for DM1C and 7.4 ‰ for DM51 at a peak temperature of 730 °C. This model demonstrates that the measured zircon core–rim and garnet $\delta^{18}O$ values reflect a change in the bulk rock of −5.1 (maximum value for DM51) to −3.7 ‰ (minimum value for DM1C), which was necessarily produced by external fluids.

In the case that DM1C and DM51 evolved in a closed system from 15 kbar, 600 °C to 40 kbar, 720 °C, the prograde variation of equilibrium $\delta^{18}O$ for the metamorphic minerals can be calculated using the modal information extracted from the Theriak data. In this way, $\delta^{18}O$ values obtained in the different zircon zones can be interpreted in terms of the evolution of the WR (Fig. 9). The DM51 modelling results differ significantly from the measured values of Sharp et al. (1993). For instance, the modelled $\delta^{18}O$ of quartz is 1.2 ‰ higher than the quartz measured by Sharp et al. (1993). The fractionation coefficient used for garnet–quartz in Zheng (1993a, b) predicts a bigger $\Delta^{18}O$ quartz–garnet than admitted in most recent

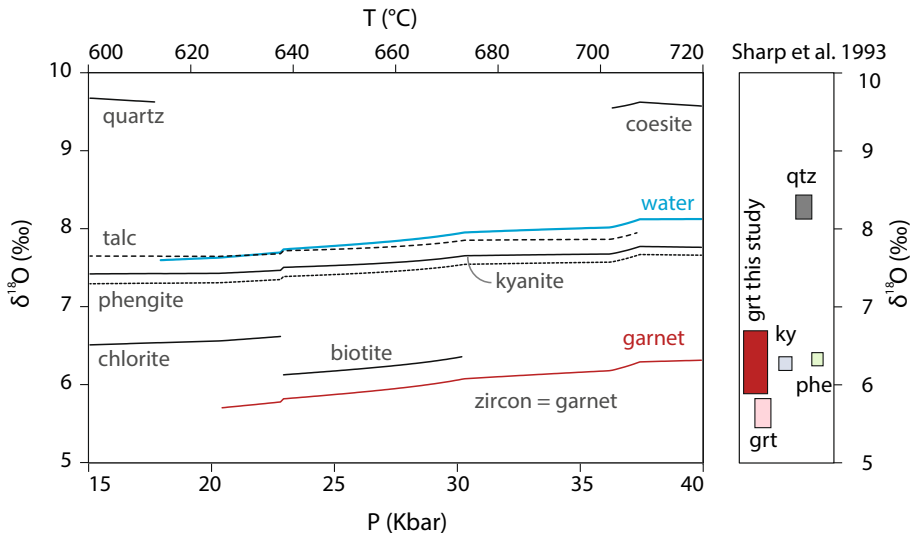

Fig. 9 Modelled oxygen isotope values for different minerals during prograde metamorphism of DM51, at a constant WR $\delta^{18}O$. The *right panel* shows the measured values for mineral composition from Sharp et al. (1993) and this study (garnet)

studies (e.g. Lackey et al. 2006; Valley 2003). This will not change the behaviour of other phases much, given the low modal abundance of quartz, but may generate an offset in the values for other phases as they are calculated from the measured garnet. Given that the $\delta^{18}O$ of garnet measured by Sharp et al. (1993) is 0.8 ‰ lower than the garnet we measured in this study, part of the observed offset could also be due to a difference in the bulk rock $\delta^{18}O$ between the two samples. As other fractionation coefficients, such as garnet–kyanite and garnet–phengite, seem to be overestimated by the increment method calculations of Zheng (1993a, b) compared to what is measured by Sharp et al. (1993), the prograde zoning modelled in minerals is likely to be of the maximum amplitude expected for this sample. Our results for DM51 (Fig. 9) show that along the prograde path, the variation in $\delta^{18}O$ expected in zircon and garnet is small, of the order of +0.6 ‰ between core and rim. 0.6 ‰ is within the analytical precision of single measurements for our analyses, so the presence of such zoning in DM51 garnet cannot be tested. Nevertheless, we observe no variation from garnet core to rim in DM51 outside analytical precision, nor in between zircon inner and outer rims. This is consistent with the constant WR hypothesis used to produce the model. In the other sample DM1C, garnet and zircon most likely crystallised close to peak pressure and temperature in a single event and are thus expected to yield homogeneous $\delta^{18}O$ signatures. Therefore, we can conclude that the oxygen isotopic composition of the UHP minerals is the product of internal metamorphic fractionation within a bulk rock with a $\delta^{18}O$ of 7.4–8.4 ‰. This $\delta^{18}O$ value is well below the protolith value of 12 ‰ and was acquired before UHP conditions. The timing and conditions of the process that led to this isotopic signature are discussed below.

Metasomatic event

Our new oxygen isotope, trace element and age data of inherited zircon combined with bulk rock compositions (Schertl and Schreyer 2008; Ferrando et al. 2009) convincingly show that the whiteschists represent a metasomatised granite. Additionally, ages of the zircon cores analysed by Gebauer et al. (1997) yield a Permian age that is identical to what is measured in the surrounding metagranite (Paquette et al. 1999), suggesting that the whiteschists have evolved from the metagranite by a metasomatic process after the crystallisation of the magmatic zircons. The context in which this fluid circulation occurred is debated (e.g. discussion in Schertl and Schreyer 2008), but a number of studies have attributed metasomatism to prograde Alpine metamorphism (Compagnoni and Hirajima 2001; Sharp and Barnes 2004; Ferrando et al. 2009).

Peak zircon, monazite and garnet (this study) as well as other metamorphic phases analysed by Sharp et al. (1993) are homogenous in $\delta^{18}O$ and have equilibrium compositions. The S-type metagranite and metasedimentary sequence that outcrop in the same unit are expected to have significantly different $\delta^{18}O$ values (metagranite ~ 12 ‰, Sharp et al. 1993) than the 7.4–8.4 ‰ of the whiteschists. The absence of measurable zoning in garnet and metamorphic zircon within the whiteschists, as predicted by constant WR modelling (Fig. 9), indicates that there was no significant fluid influx into the whiteschist from either the metagranite or metasediments at conditions where garnet was stable, i.e. HP to UHP. On the other hand, Vielzeuf et al. (2005) documented oxygen isotope zoning in a garnet within the paragneiss surrounding the whiteschists, which is similar to the superzoned garnet of Compagnoni and Hirajima (2001). Vielzeuf et al. (2005) measured an almandine core at 7.5–8.0 ‰ and a thin pyrope rim at 5.0–5.5 ‰

and attributed this to high-pressure overgrowth. This result can be interpreted as the late HP–UHP influx of a fluid derived from the neighbouring whiteschists layers into the gneiss.

The oxygen results together with the thermodynamic modelling indicate that during high pressure metamorphism fluids in the whiteschists were internally derived and that these rocks had already acquired their Mg-rich and low $\delta^{18}O$ signature. Therefore, we conclude that the main metasomatic event that caused the granite to whiteschist transformation occurred prior to HP–UHP metamorphism, that is before a significant dehydration reaction modelled in the whiteschists at ~22kbar, 640 °C which produced the first garnet (Prp I in Ferrando et al. 2009). This is consistent with the fluid inclusion data in the whiteschist lens (Compagnoni and Hirajima 2001; Ferrando et al. 2009), suggesting that metasomatism occurred before the growth of the Prp I. It has been suggested that metasomatism of the whiteschists occurred early on the prograde metamorphic path and was the result of serpentinite dehydration in the lower levels of the slab during initial subduction (Compagnoni and Hirajima 2001; Ferrando 2012). This scenario is difficult to reconcile with the observation that the gneisses surrounding the whiteschist appear unaffected by such external fluid influx. Instead, the available data suggest that the gneisses were locally infiltrated by fluids that derive from the whiteschists (Vielzeuf et al. 2005). Therefore, it seems more feasible that the alteration of the S-type granite occurred prior to subduction. Franz et al. (2013) compiled worldwide occurrences of whiteschists and looked at potential protolith formation. They concluded that the best explanation for the Dora-Maira whiteschists is a chemical weathering to produce a kaolinite–chlorite-rich protolith. In context of the tectonic evolution between Permian intrusion and Alpine high-pressure metamorphism, the simplest explanation is that the S-type granites were metasomatised in an oceanic environment, where large fluid/rock ratios can achieve significant shifts in $\delta^{18}O$. We speculate that the continental sequence and S-type granite of the Dora-Maira were a continental sliver that was part of a hyper-extended margin during the well-documented Jurassic rifting episode, as reconstructed by Beltrando et al. (2010). Focussed circulation of seawater along shear zones is common in submerged extensional settings, such as rifting or oceanic spreading when a high thermal gradient is present (e.g. McCaig et al. 2007). Such localised fluid–rock interaction could lead to a kaolinite/muscovite/chlorite alteration. From the modelled chlorite ($\delta^{18}O$ ~ 6.5) and phengite ($\delta^{18}O$ ~ 7.3) oxygen isotopes at 15 kbar, 600 °C, we can infer that the hydrothermal fluid acting at $T \leq 350$ °C had a $\delta^{18}O$ of maximum 7 ‰ (more likely < 7 ‰). This scenario is also supported by the occurrence of similar whiteschists lithologies in the same tectonic setting along the Alpine orogeny (review in Ferrando 2012).

Conclusions

The systematic study at the microscale of garnet, zircon and monazite compositions and oxygen isotopes together with age constraints from the accessory minerals allows reconstruction of a detailed P–T–time–fluid path for the Dora-Maira UHP whiteschists. Zircon growth during prograde metamorphism is related to fluid pulses in the whiteschists due to the breakdown of chlorite and talc. Fluid circulation led to the partial dissolution of inherited, U-rich, metamict zircon cores and the precipitation of metamorphic rims. The cavities resulting from zircon dissolution were filled with metamorphic phases and fluids. The tight link between metamorphic reactions and zircon recrystallisation allows constraining subduction rates of the Dora-Maira Massif. Prograde (~ 22 kbar) and peak zircon rims (35–40 kbar), as well as peak monazite (35–40 kbar in DM1C) have undistinguishable ages of 34.5 ± 0.7 to 35.1 ± 0.5 Ma, implying a prograde subduction rate of a few cm/yr between ~22 and 35 kbar. Garnet, zircon and monazite yield $\delta^{18}O$ values of 6–7 ‰, within error identical for temperatures of 700 °C—implying close to 0 ‰ fractionation at this temperature between these minerals. It is concluded that, in order to reach these $\delta^{18}O$ values, an external fluid with a low $\delta^{18}O$ of at most 7 ‰ metasomatised the original S-type granite into the Mg-rich whiteschists. Moreover, there is no evidence for external fluid input during HP to UHP metamorphism of the whiteschists. We conclude that the significant metasomatic event that affected the original granite occurred by seafloor alteration during Permian extension.

Acknowledgments This study benefited from the technical support of R Rapp for electron microprobe analysis. L Gauthiez-Putallaz acknowledges L Martin for providing SIMS garnet standard PrpDM. D Rubatto acknowledges the financial support of the Australia Research Council, DP110101599.

References

Aleinikoff JN, Schenck WS, Plank MO, Srogi L, Fanning M, Kamo SL, Bosbyshell H (2006) Deciphering igneous and metamorphic events in high-grade rocks of the Wilmington Complex, Delaware: Morphology, cathodoluminescence and backscattered electron zoning, and SHRIMP U-Pb geochronology of zircon and monazite. Geol Soc Am Bull 118:39–64. doi:10.1130/B25659.1

Amato JM, Johnson CM, Baumgartner LP, Beard BL (1999) Rapid exhumation of the Zermatt–Saas ophiolite deduced from high-precision SmNd and RbSr geochronology. Earth Planet Sci Lett 171:425–438

Beltrando M, Rubatto D, Manatschal G (2010) From passive margins to orogens: the link between ocean-continent transition zones and (ultra) high-pressure metamorphism. Geology 38:559–562

Black LP, Kamo SL, Allen CM, Aleinikoff JN, Davis DW, Korsch RJ, Foudoulis C (2003) TEMORA 1: a new zircon standard for Phanerozoic U–Pb geochronology. Chem Geol 200:155–170. doi:10.1016/S0009-2541(03)00165-7

Black LP, Kamo SL, Allen CM, Davis DW, Aleinikoff JN, Valley JW, Mundil R, Campbell IH, Korsch RJ, Williams IS, Foudoulis C (2004) Improved 206 Pb/238 U microprobe geochronology by the monitoring of a trace-element-related matrix effect; SHRIMP, ID–TIMS, ELA–ICP–MS and oxygen isotope documentation for a series of zircon standards. Chem Geol 205:115–140

Breecker DO, Sharp ZD (2007) A monazite oxygen isotope thermometer. Am Mineral 92:1561–1572

Carry N, Gueydan F, Marquer D, Brun JP (2011) HP–UHP metamorphism as an indicator of slab dip variations in the Alpine arc. Int J Earth Sci 100:1087–1094

Chopin C (1984) Coesite and pure pyrope in high-grade blueschists of the western alps—a 1st record and some consequences. Contrib Mineral Petrol 86:107–118. doi:10.1007/Bf00381838

Chopin C, Monié P (1984) A unique magnesiochloritoid-bearing, high-pressure assemblage from the Monte-Rosa, western alps—petrologic and Ar-40–Ar-39 radiometric study. Contrib Mineral Petrol 87:388–398. doi:10.1007/Bf00381295

Chopin C, Schertl HP (1999) The UHP unit in the Dora-Maira massif. Western Alps Int Geol Rev 41:765–780

Coggon R, Holland T (2002) Mixing properties of phengitic micas and revised garnet-phengite thermobarometers. J Metamorph Geol 20:683–696

Compagnoni R, Hirajima T (2001) Superzoned garnets in the coesite-bearing Brossasco-Isasca Unit, Dora-Maira massif, Western Alps, and the origin of the whiteschists. Lithos 57:219–236. doi:10.1016/S0024-4937(01)00041-X

Compagnoni R, Rolfo F, Groppo C, Hirajima T, Turello R (2012) Geological map of the ultra-high pressure Brossasco-Isasca unit (Western Alps, Italy). J Maps 8:465–472

de Capitani C, Petrakakis K (2010) The computation of equilibrium assemblage diagrams with Theriak/Domino software. Am Mineral 95:1006–1016

Dragovic B, Samanta LM, Baxter EF, Selverstone J (2012) Using garnet to constrain the duration and rate of water-releasing metamorphic reactions during subduction: an example from Sifnos, Greece. Chem Geol 314:9–22. doi:10.1016/j.chemgeo.2012.04.016

Duchêne S, Blichert-Toft J, Luais B, Télouk P, Lardeaux JM, Albarede F (1997) The Lu-Hf dating of garnets and the ages of the Alpine high-pressure metamorphism. Nature 387:586–589

Eggins S, Kinsley L, Shelley J (1998) Deposition and element fractionation processes during atmospheric pressure laser sampling for analysis by ICP-MS. Appl Surf Sci 127:278–286

Ferrando S (2012) Mg-metasomatism of metagranitoids from the Alps: genesis and possible tectonic scenarios. Terra Nova 24:423–436

Ferrando S, Frezzotti ML, Petrelli M, Compagnoni R (2009) Metasomatism of continental crust during subduction: the UHP whiteschists from the Southern Dora-Maira Massif (Italian Western Alps). J Metamorph Geol 27:739–756. doi:10.1111/j.1525-1314.2009.00837.x

Ford M, Duchêne S, Gasquet D, Vanderhaeghe O (2006) Two-phase orogenic convergence in the external and internal SW Alps. J Geol Soc Lond 163:815–826

Franz L, Romer RL, de Capitani C (2013) Protoliths and phase petrology of whiteschists. Contrib Mineral Petrol 166:255–274

Frezzotti M, Selverstone J, Sharp Z, Compagnoni R (2011) Carbonate dissolution during subduction revealed by diamond-bearing rocks from the Alps. Nat Geosci 4:703–706

Gebauer D, Schertl HP, Brix M, Schreyer W (1997) 35 Ma old ultrahigh-pressure metamorphism and evidence for very rapid exhumation in the Dora Maira Massif, Western Alps. Lithos 41:5–24. doi:10.1016/S0024-4937(97)82002-6

Geisler T, Schaltegger U, Tomaschek F (2007) Re-equilibration of zircon in aqueous fluids and melts. Elements 3:43–50

Gilotti J (2013) The realm of ultrahigh-pressure metamorphism. Elements 9:255–260. doi:10.2113/gselements.9.4.255

Grevel C, Schreyer W, Grevel KD, Schertl HP, Willner AP (2009) REE distribution, mobilization and fractionation in the coesite-bearing 'pyrope quartzite' and related rocks of the Dora-Maira Massif, Western Alps. Eur J Mineral 21:1213–1224. doi:10.1127/0935-1221/2009/0021-1967

Hermann J (2003) Experimental evidence for diamond-facies metamorphism in the Dora-Maira massif. Lithos 70:163–182. doi:10.1016/S0024-4937(03)00097-5

Hermann J, Rubatto D (2003) Relating zircon and monazite domains to garnet growth zones: age and duration of granulite facies metamorphism in the Val Malenco lower crust. J Metamorph Geol 21:833–852

Hermann J, Rubatto D (2014) 4.9—subduction of continental crust to mantle depth: geochemistry of ultrahigh-pressure rocks Treatise on geochemistry, 2nd edn. Elsevier, Oxford, pp 309–340

Hermann J, Rubatto D, Korsakov A, Shatsky VS (2001) Multiple zircon growth during fast exhumation of diamondiferous, deeply subducted continental crust (Kokchetav Massif, Kazakhstan). Contrib Mineral Petrol 141:66–82

Holland T, Powell R (1998) An internally consistent thermodynamic data set for phases of petrological interest. J Metamorph Geol 16:309–343

Hoskin PW, Schaltegger U (2003) The composition of zircon and igneous and metamorphic petrogenesis. Rev Mineral Geochem 53:27–62

Hu G, Clayton RN (2003) Oxygen isotope salt effects at high pressure and high temperature and the calibration of oxygen isotope geothermometers. Geochim Cosmochim Acta 67:3227–3246

Ickert R et al (2008) Determining high precision, in situ, oxygen isotope ratios with a SHRIMP II: analyses of MPI-DING silicate-glass reference materials and zircon from contrasting granites. Chem Geol 257:114–128

Jeon H, Williams IS, Chappell BW (2012) Magma to mud to magma: rapid crustal recycling by Permian granite magmatism near the eastern Gondwana margin. Earth Planet Sci Lett 319–320:104–117. doi:10.1016/j.epsl.2011.12.010

John T, Gussone N, Podladchikov YY, Bebout GE, Dohmen R, Halama R, Klemd R, Magna T, Seitz HM (2012) Volcanic arcs fed by rapid pulsed fluid flow through subducting slabs. Nat Geosci 5:489–492

Kohn MJ (1993) Modeling of prograde mineral $\delta^{18}O$ changes in metamorphic systems. Contrib Mineral Petrol 113:249–261

Kohn MJ, Corrie SL, Markley C (2015) The fall and rise of metamorphic zircon. Am Mineral 100:897–908

Kylander-Clark AR, Hacker BR, Mattinson CG (2012) Size and exhumation rate of ultrahigh-pressure terranes linked to orogenic stage. Earth Planet Sci Lett 321:115–120

Lackey JS, Valley JW, Hinke HJ (2006) Deciphering the source and contamination history of peraluminous magmas using $\delta^{18}O$ of accessory minerals: examples from garnet-bearing plutons of the Sierra Nevada batholith. Contrib Mineral Petrol 151:20–44

Lackey JS, Valley JW, Chen JH, Stockli DF (2008) Dynamic magma systems, crustal recycling, and alteration in the central Sierra Nevada batholith: the oxygen isotope record. J Petrol 49:1397–1426

Lapen TJ, Johnson CM, Baumgartner LP, Mahlen NJ, Beard BL, Amato JM (2003) Burial rates during prograde metamorphism of an ultra-high-pressure terrane: an example from Lago di Cignana, western Alps, Italy. Earth Planet Sci Lett 215:57–72

Liu F, Liou J (2011) Zircon as the best mineral for P-T–time history of UHP metamorphism: a review on mineral inclusions and U–Pb SHRIMP ages of zircons from the Dabie-Sulu UHP rocks. J Asian Earth Sci 40:1–39

Ludwig K (2009) SQUID 2 (rev. 2.50): A user's manual. Berkeley Geochronology Center Spec Pub 5, 104 p

Ludwig K (2012) User's manual for Isoplot 3.75. A geochronological toolkit for microsoft excel. Berkeley Geochronology Center Spec Pub 5, 75 p

Manning CE (2004) The chemistry of subduction-zone fluids. Earth Planet Sci Lett 223:1–16

Martin LA, Rubatto D, Vitale Brovarone A, Hermann J (2011) Late Eocene lawsonite-eclogite facies metasomatism of a granulite sliver associated to ophiolites in Alpine Corsica. Lithos 125:620–640

Martin LA, Rubatto D, Crépisson C, Hermann J, Putlitz B, Vitale-Brovarone A (2014) Garnet oxygen analysis by SHRIMP-SI: matrix corrections and application to high-pressure metasomatic rocks from Alpine Corsica. Chem Geol 374:25–36

McCaig AM, Cliff RA, Escartin J, Fallick AE, MacLeod CJ (2007) Oceanic detachment faults focus very large volumes of black smoker fluids. Geology 35:935–938

Otamendi JE, Jesús D, Douce AEP, Castro A (2002) Rayleigh fractionation of heavy rare earths and yttrium during metamorphic garnet growth. Geology 30:159–162

Page F, Kita NT, Valley JW (2010) Ion microprobe analysis of oxygen isotopes in garnets of complex chemistry. Chem Geol 270:9–19

Page FZ, Essene EJ, Mukasa SB, Valley JW (2014) A garnet-zircon oxygen isotope record of subduction and exhumation fluids from the Franciscan complex, California. J Petrol 55:103–131. doi:10.1093/petrology/egt062

Paquette JL, Montel JM, Chopin C (1999) U-Th-Pb dating of the Brossasco ultrahigh-pressure metagranite, Dora-Maira massif, western Alps. Eur J Mineral 11:69–77

Paton C, Hellstrom J, Paul B, Woodhead J, Hergt J (2011) Iolite: freeware for the visualisation and processing of mass spectrometric data. J Anal At Spectrom 26:2508–2518

Philippot P, Chevalier P, Chopin C, Debussy J (1995) Fluid composition and evolution in coesite-bearing rocks (Dora-Maira massif, Western Alps): implications for element recycling during subduction. Contrib Mineral Petrol 121:29–44

Philippot P, Blichert-Toft J, Perchuk A, Costa S, Gerasimov V (2001) Lu–Hf and Ar–Ar chronometry supports extreme rate of subduction zone metamorphism deduced from geospeedometry. Tectonophysics 342:23–38

Pollington AD, Baxter EF (2010) High resolution Sm-Nd garnet geochronology reveals the uneven pace of tectonometamorphic processes. Earth Planet Sci Lett 293:63–71. doi:10.1016/j.epsl.2010.02.019

Rizvanova N et al (2000) Zircon reaction and stability of the U–Pb isotope system during interaction with carbonate fluid: experimental hydrothermal study. Contrib Mineral Petrol 139:101–114

Rubatto D (2002) Zircon trace element geochemistry: partitioning with garnet and the link between U–Pb ages and metamorphism. Chem Geol 184:123–138. doi:10.1016/S0009-2541(01)00355-2

Rubatto D, Angiboust S (2015) Oxygen isotope record of oceanic and high-pressure metasomatism: a P–T–time–fluid path for the Monviso eclogites (Italy). Contrib Mineral Petrol 170:44

Rubatto D, Hermann J (2001) Exhumation as fast as subduction? Geology 29:3–6

Rubatto D, Hermann J (2003) Zircon formation during fluid circulation in eclogites (Monviso, Western Alps): implications for Zr and Hf budget in subduction zones. Geochim Cosmochim Acta 67:2173–2187. doi:10.1016/S0016-7037(02)01321-2

Rubatto D, Hermann J (2007) Experimental zircon/melt and zircon/garnet trace element partitioning and implications for the geochronology of crustal rocks. Chem Geol 241:38–61. doi:10.1016/j.chemgeo.2007.01.027

Rubatto D, Muntener O, Barnhoorn A, Gregory C (2008) Dissolution-reprecipitation of zircon at low-temperature, high-pressure conditions (Lanzo Massif, Italy). Am Mineral 93:1519–1529. doi:10.2138/Am.2008.2874

Rubatto D, Putlitz B, Gauthiez-Putallaz L, Crépisson C, Buick IS, Zheng Y-F (2014) Measurement of in situ oxygen isotope ratios in monazite by SHRIMP ion microprobe: standards, protocols and implications. Chem Geol 380:84–96. doi:10.1016/j.chemgeo.2014.04.029

Schärer U (1984) The effect of initial ^{230}Th disequilibrium on young UPb ages: the Makalu case, Himalaya. Earth Planet Sci Lett 67:191–204

Schertl HP, Schreyer W (1996) Mineral inclusions in heavy minerals of the ultrahigh-pressure metamorphic rocks of the Dora-Maira Massif and their bearing on the relative timing of the petrological events. Earth process: reading the isotopic code. pp 331–342

Schertl HP, Schreyer W (2008) Geochemistry of coesite-bearing "pyrope quartzite" and related rocks from the Dora-Maira Massif, Western Alps. Eur J Mineral 20:791–809. doi:10.1127/0935-1221/2008/0020-1862

Schertl HP, Schreyer W, Chopin C (1991) The pyrope-coesite rocks and their country rocks at Parigi, Dora Maira Massif, Western Alps—detailed petrography, mineral chemistry and Pt-Path. Contrib Mineral Petrol 108:1–21. doi:10.1007/Bf00307322

Schmidt A, Mezger K, O'Brien PJ (2011) The time of eclogite formation in the ultrahigh pressure rocks of the Sulu terrane: constraints from Lu–Hf garnet geochronology. Lithos 125:743–756

Schreyer W (1973) Whiteschist: a high-pressure rock and its geologic significance. J Geol 81:735–739

Sharp Z, Barnes J (2004) Water-soluble chlorides in massive seafloor serpentinites: a source of chloride in subduction zones. Earth Planet Sci Lett 226:243–254

Sharp ZD, Essene EJ, Hunziker JC (1993) Stable isotope geochemistry and phase equilibria of coesite-bearing whiteschists, Dora Maira Massif, western Alps. Contrib Mineral Petrol 114:1–12. doi:10.1007/bf00307861

Simon G, Chopin C, Schenk V (1997) Near-end-member magnesiochloritoid in prograde-zoned pyrope, Dora-Maira massif, western Alps. Lithos 41:37–57. doi:10.1016/S0024-4937(97)82004-X

Skora S, Mahlen NJ, Johnson CM, Baumgartner LP, Lapen TJ, Beard BL, Szilvagyi ET (2015) Evidence for protracted prograde metamorphism followed by rapid exhumation of the Zermatt-Saas Fee ophiolite. J Metamorph Geol 33:711–734

Stacey JS, Kramers JD (1975) Approximation of terrestrial lead evolution by a two-stage model. Earth Planet Sci Lett 26:207–221

Sun S-S, McDonough W (1989) Chemical and isotopic systematics of oceanic basalts: implications for mantle composition and processes. Geol Soc Lond Special Publ 42:313–345

Tatsumi Y, Eggins S (1995) Subduction zone magmatism, vol 1. Blackwell Science, Cambridge

Tilton GR, Schreyer W, Schertl HP (1991) Pb–Sr–Nd isotopic behavior of deeply subducted crustal rocks from the Dora Maira Massif, Western Alps, Italy-Ii—what is the age of the ultrahigh-pressure metamorphism. Contrib Mineral Petrol 108:22–33. doi:10.1007/Bf00307323

Tomaschek F, Kennedy AK, Villa IM, Lagos M, Ballhaus C (2003) Zircons from Syros, Cyclades, Greece—recrystallization and mobilization of zircon during high-pressure metamorphism. J Petrol 44:1977–2002

Trail D, Bindeman IN, Watson EB, Schmitt AK (2009) Experimental calibration of oxygen isotope fractionation between quartz and zircon. Geochim Cosmochim Acta 73:7110–7126

Vaggelli G, Borghi A, Cossio R, Fedi M, Giuntini L, Lombardo B, Marino A, Massi M, Olmi F, Petrelli M (2006) Micro-PIXE

analysis of monazite from the Dora Maira massif, western Italian Alps. Microchim Acta 155:305–311

Valley JW (2003) Oxygen isotopes in zircon. Rev Mineral Geochem 53:343–385

Valley JW, Kitchen N, Kohn MJ, Niendorf CR, Spicuzza MJ (1995) UWG-2, a garnet standard for oxygen isotope ratios: strategies for high precision and accuracy with laser heating. Geochim et Cosmochim Acta 59:5223–5231

Vielzeuf D, Champenois M, Valley JW, Brunet F, Devidal J (2005) SIMS analyses of oxygen isotopes: matrix effects in Fe–Mg–Ca garnets. Chem Geol 223:208–226

White R, Powell R, Clarke G (2002) The interpretation of reaction textures in Fe-rich metapelitic granulites of the Musgrave Block, central Australia: constraints from mineral equilibria calculations in the system K_2O–FeO–MgO–Al_2O_3–SiO_2–H_2O–TiO_2–Fe_2O_3. J Metamorph Geol 20:41–55

White R, Powell R, Holland T (2007) Progress relating to calculation of partial melting equilibria for metapelites. J Metamorph Geol 25:511–527

Williams IS (1998) U–Th–Pb geochronology by ion microprobe. Rev Econ Geol 7:1–35

Woodhead JD, Hellstrom J, Hergt JM, Greig A, Maas R (2007) Isotopic and elemental imaging of geological materials by laser ablation inductively coupled plasma-mass spectrometry. Geostand Geoanal Res 31:331–343

Zhang Z-M, Shen K, Sun W-D, Liu Y-S, Liou J, Shi C, Wang J-L (2008) Fluids in deeply subducted continental crust: petrology, mineral chemistry and fluid inclusion of UHP metamorphic veins from the Sulu orogen, eastern China. Geochim Cosmochim Acta 72:3200–3228

Zhang Z, Schertl HP, Wang J, Shen K, Liou J (2009) Source of coesite inclusions within inherited magmatic zircon from Sulu UHP rocks, eastern China, and their bearing for fluid–rock interaction and SHRIMP dating. J Metamorph Geol 27:317–333

Zheng Y-F (1993a) Calculation of oxygen isotope fractionation in anhydrous silicate minerals. Geochim Cosmochim Acta 57:1079–1091

Zheng Y-F (1993b) Calculation of oxygen isotope fractionation in hydroxyl-bearing silicates. Earth Planet Sci Lett 120:247–263

Zheng Y-F (2009) Fluid regime in continental subduction zones: petrological insights from ultrahigh-pressure metamorphic rocks. J Geol Soc Lond 166:763–782

Zheng Y-F, Fu B, Gong B, Li L (2003) Stable isotope geochemistry of ultrahigh pressure metamorphic rocks from the Dabie-Sulu orogen in China: implications for geodynamics and fluid regime. Earth Sci Rev 62:105–161